Cell

Intestinal Tumorigenesis Initiated by Dedifferentiation and Acquisition of Stem-Cell-like Properties

Sarah Schwitalla,[1] Alexander A. Fingerle,[2] Patrizia Cammareri,[5] Tim Nebelsiek,[1] Serkan I. Göktuna,[1] Paul K. Ziegler,[1] Ozge Canli,[1] Jarom Heijmans,[6] David J. Huels,[5] Guenievre Moreaux,[5] Rudolf A. Rupec,[7] Markus Gerhard,[3] Roland Schmid,[4] Nick Barker,[9] Hans Clevers,[10] Roland Lang,[11] Jens Neumann,[8] Thomas Kirchner,[8] Makoto M. Taketo,[12] Gijs R. van den Brink,[6] Owen J. Sansom,[5] Melek C. Arkan,[1] and Florian R. Greten[1,*]

[1]Institute of Molecular Immunology, Klinikum rechts der Isar
[2]Department of Radiology, Klinikum rechts der Isar
[3]Institute of Medical Microbiology, Immunology and Hygiene
[4]2nd Department of Medicine, Klinikum rechts der Isar
Technische Universität München, 81675 Munich, Germany
[5]Beatson Institute for Cancer Research, Glasgow G61 1BD, UK
[6]Tytgat Institute for Liver and Intestinal Research, Academic Medical Centre, 1105 BK Amsterdam, Netherlands
[7]Department of Dermatology and Allergology
[8]Institute of Pathology
Ludwig-Maximilians-University, 80337 Munich, Germany
[9]Institute of Medical Biology, 8A Biomedical Grove, 06-06 Immunos, Singapore 138648, Singapore
[10]Hubrecht Institute for Developmental Biology and Stem Cell Research and University Medical Centre Utrecht, 3584CT Utrecht, Netherlands
[11]Institute of Clinical Microbiology, Immunology and Hygiene, University Hospital Erlangen, 91054 Erlangen, Germany
[12]Department of Pharmacology, Graduate School of Medicine, Kyoto University, Kyoto 606-8501, Japan
*Correspondence: florian.greten@lrz.tum.de
http://dx.doi.org/10.1016/j.cell.2012.12.012

SUMMARY

Cell-type plasticity within a tumor has recently been suggested to cause a bidirectional conversion between tumor-initiating stem cells and nonstem cells triggered by an inflammatory stroma. NF-κB represents a key transcription factor within the inflammatory tumor microenvironment. However, NF-κB's function in tumor-initiating cells has not been examined yet. Using a genetic model of intestinal epithelial cell (IEC)-restricted constitutive Wnt-activation, which comprises the most common event in the initiation of colon cancer, we demonstrate that NF-κB modulates Wnt signaling and show that IEC-specific ablation of RelA/p65 retards crypt stem cell expansion. In contrast, elevated NF-κB signaling enhances Wnt activation and induces dedifferentiation of nonstem cells that acquire tumor-initiating capacity. Thus, our data support the concept of bidirectional conversion and highlight the importance of inflammatory signaling for dedifferentiation and generation of tumor-initiating cells in vivo.

INTRODUCTION

The transition of an intestinal epithelial cell (IEC) into a fully transformed metastatic intestinal cancer cell follows a series of activating and inactivating mutations in various oncogenes and tumor suppressors, respectively (Fearon, 2011). The initiating event of intestinal carcinogenesis is most commonly caused by activating mutations in the Wnt-pathway (i.e., in *APC* or *CTNNB*), that lead to stabilization of β-catenin and subsequent constitutive transcription by a β-catenin/Tcf complex (Bienz and Clevers, 2000). This triggers expansion and transformation of the stem cell compartment and leads subsequently to the development of adenomatous polyps (van de Wetering et al., 2002). During the course of tumorigenesis, additional mutations in other oncogenes and tumor suppressors such as *KRAS* and *TP53* are usually acquired (Fearon, 2011). In the untransformed intestine, two types of multipotent stem cells have been identified: the first comprises a population of rapidly cycling cells at the crypt base expressing the Wnt-target gene leucine-rich-repeat-containing G protein coupled receptor 5 (Lgr5) (Barker et al., 2007). The second pool consists of quiescent Bmi1-expressing cells that can mostly be found above the crypt base (Sangiorgi and Capecchi, 2008) and that have the capacity to regenerate $Lgr5^+$ cells upon tissue injury (Tian et al., 2011). Because of the frequent observation that very early adenomatous polyps are found at the top of colonic crypts without any contact to the stem cell compartment (Cole and McKalen, 1963) the so-called "top-down model of adenoma morphogenesis" has been suggested (Shih et al., 2001). However, recent genetic evidence provided support for the "bottom-up histogenesis" (Preston et al., 2003) when it was shown that $Lgr5^+$ or $Bmi1^+$ stem cells can act as the cells of origin of intestinal cancer in mice (Barker et al., 2009; Sangiorgi and Capecchi, 2008).

Various forms of chronic inflammation increase the risk of several common cancers (Grivennikov et al., 2010). Moreover,

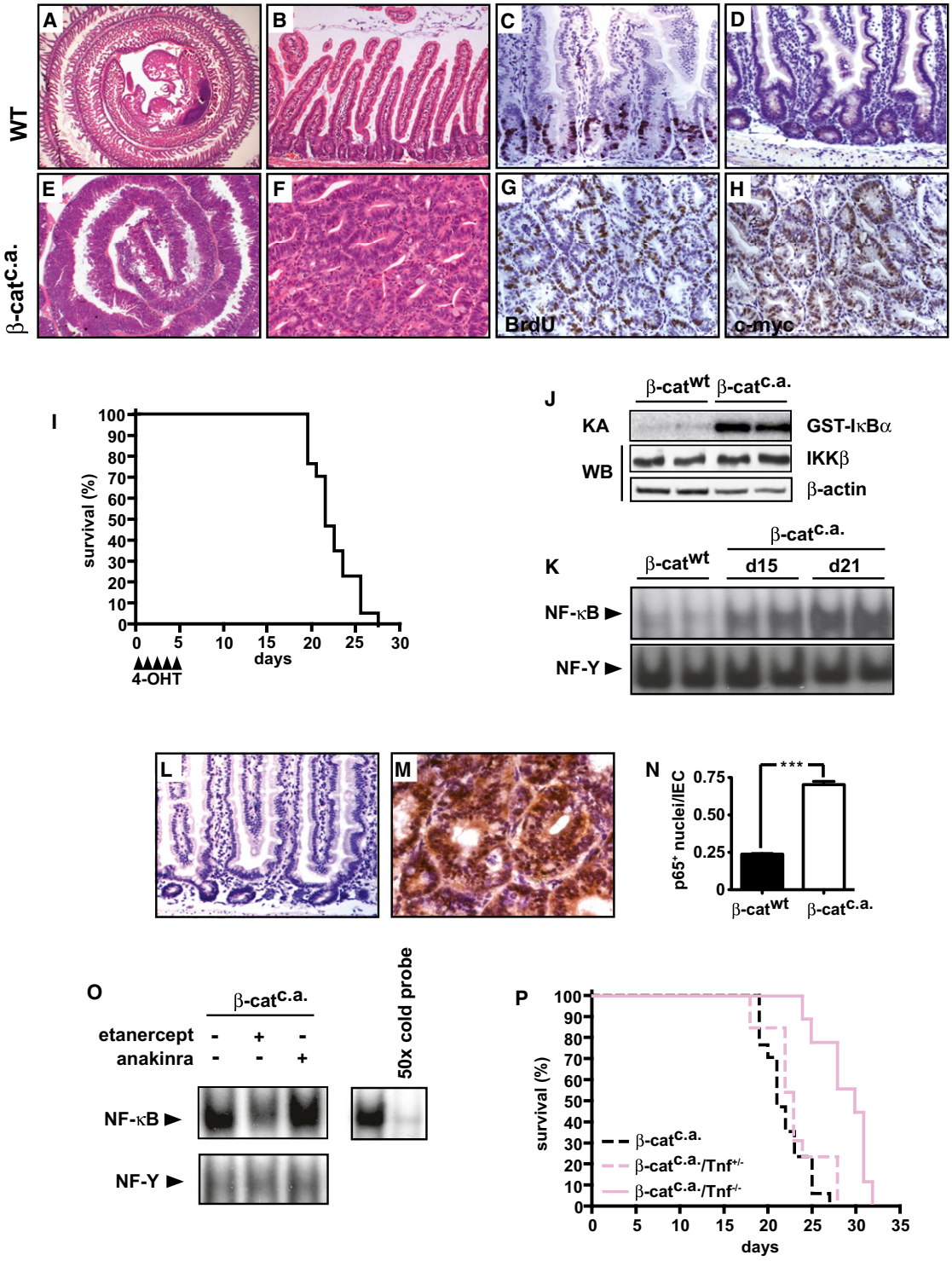

Figure 1. Stabilization of β-Catenin in IEC Induces Stem Cell Expansion and NF-κB Activation

(A–H) Representative H&E stained sections (A, B, E, and F) as well as immunohistochemical stainings (C, D, G, and H) of small intestines from unchallenged wild-type (A–D) or *β-cat*$^{c.a.}$ mice (E–H) 25 days after the first tamoxifen administration.

(I) Kaplan-Meier survival curve of *β-cat*$^{c.a.}$ mice.

(J) Elevated IκB-kinase activity in IEC of *β-cat*$^{c.a.}$ mice 21 days after tamoxifen administration.

(K) NF-κB binding activity in IEC of *β-cat*$^{c.a.}$ mice 15 or 21 days after tamoxifen administration.

(L and M) Immunohistochemical staining of RelA/p65 in wild-type (L) and *β-cat*$^{c.a.}$ mice (M).

(legend continued on next page)

long-term administration of nonsteroidal anti-inflammatory drugs (NSAIDs) such as aspirin can be tumor preventive and significantly reduce incidence of many solid tumor entities, including colorectal cancer (Rothwell et al., 2011), suggesting a specific effect of low-grade inflammation in this context. However, the exact mechanisms by which NSAIDS can provide chemoprevention remain to be defined. The transcription factor NF-κB, a master regulator of cell survival, inflammation, and immunity, has been shown to comprise a key link between inflammation and cancer (Karin and Greten, 2005). First, genetic evidence came from a mouse model of colitis-associated cancer, where IκB-kinase (IKK)β-dependent NF-κB activity in IEC promoted survival of initiated cells, whereas in myeloid cells it controlled the transcription of genes encoding proinflammatory cytokines that can stimulate proliferation in a paracrine manner (Greten et al., 2004). Additional proof for NF-κB's direct and indirect effects on tumor promotion and progression has originated from several animal models of hepatocellular carcinoma, gastric cancer, and lung cancer (Bollrath and Greten, 2009). The canonical NF-κB activation pathway is triggered by a variety of stimuli including TNF-α, IL-1β, and pathogen-associated molecular patterns (PAMPs), which upon binding to their respective receptors activate the IKK complex. As a consequence, IKK phosphorylates NF-κB-bound IκBs and targets them for ubiquitin-dependent degradation, thus allowing liberated NF-κB dimers to enter the nucleus. In case of the canonical NF-κB activation, this mainly depends on the IKKγ and IKKβ subunits of the IKK complex (Bollrath and Greten, 2009).

Although there is substantial evidence for a role of NF-κB in tumor promotion and progression, so far its contribution to tumor initiation and epithelial tumor stem cell function has not been addressed. Here, we demonstrate that NF-κB can enhance Wnt-signaling leading to the dedifferentiation of epithelial non-stem cells into tumor-initiating cells.

RESULTS

Constitutive Activation of β-Catenin in IEC Results in Rapid Expansion of Intestinal Crypt Stem Cells and TNFα-Dependent NF-κB Activation

To directly examine Wnt-dependent tumor initiation, we used a mouse model with a tamoxifen-inducible and conditional stable expression of β-catenin in IEC (*villin-cre*ER^{T2}/*Ctnnb*$^{loxEx3/WT}$, termed *β-cat*$^{c.a.}$). Upon oral tamoxifen gavage, Cre recombination was induced in all intestinal epithelial compartments including stem cells. This led to excision of exon 3 of *Ctnnb*, thereby resulting in a stabilized protein, which fails to undergo GSK3β-mediated degradation (Harada et al., 1999). As a consequence, β-catenin became constitutively active in IEC, which resulted in an almost complete loss of differentiated, absorptive enterocytes and a massive expansion of highly proliferative crypt stem cells that expressed high levels of the Wnt target *c-myc* (Figures 1A–1H). Following tamoxifen administration *β-cat*$^{c.a.}$ mice showed signs of severe weight loss and succumbed to the intestinal transformation within 27 days (Figure 1I). Notably, IκB kinase activity (Figure 1J) as well as NF-κB-binding activity was markedly elevated in isolated IEC (Figure 1K), whereas immunohistochemical analysis demonstrated nuclear accumulation of RelA/p65 in expanded crypt cells of *β-cat*$^{c.a.}$ mice (Figures 1L–1N). TNFα and IL-1β are considered two of the most common upstream activators of NF-κB signaling in inflammatory diseases and tumors (Karin and Greten, 2005). To examine whether these cytokines were responsible for the observed NF-κB activation in *β-cat*$^{c.a.}$ mice, we pharmacologically inhibited TNFα and IL-1β by using etanercept and anakinra, respectively. Although inhibition of TNFα markedly reduced NF-κB binding, blockade of IL-1β had no effect (Figure 1O) and loss of *Tnf* significantly prolonged survival of *β-cat*$^{c.a.}$ mice (median survival 23 days in *β-cat*$^{c.a.}$/*Tnf*$^{+/-}$ mice versus 30 days in *β-cat*$^{c.a.}$/*Tnf*$^{-/-}$ mice; Figure 1P). Collectively, these results indicate that extrinsic factors, such as TNFα, that act in a paracrine and/or autocrine manner induce classical NF-κB activation in *β-cat*$^{c.a.}$ IEC.

Inhibition of NF-κB in IEC Prolongs Survival and Delays Crypt Transformation in *β-cat*$^{c.a.}$ Mice

To directly examine whether NF-κB activity in IEC was causally involved in the expansion of intestinal crypt cells and decreased survival, we crossed floxed *Rela* animals to *β-cat*$^{c.a.}$ mice. Indeed, loss of RelA/p65 function specifically in IEC significantly prolonged survival of *β-cat*$^{c.a.}$ mice by 50% (median survival 22 days in *β-cat*$^{c.a.}$/*Rela*$^{lox/WT}$ mice versus 33 days in *β-cat*$^{c.a.}$/*Rela*$^{\Delta IEC}$ mice; Figure 2A). This effect was even more pronounced than whole-body deletion of *Tnf*, indicating that apart from TNFα also other upstream activators can signal to NF-κB in *β-cat*$^{c.a.}$ mice. Because *β-cat*$^{c.a.}$/*Rela*$^{\Delta IEC}$ compound mutants were histologically comparable to single *β-cat*$^{c.a.}$ mice in terms of proliferation and apoptosis index at their respective time of death (data not shown), we examined mice of both genotypes 15 days after the first tamoxifen treatment, 5 days before the death of the first *β-cat*$^{c.a.}$ animal.

Also at this time point, no difference in the number of apoptotic cells was detected (data not shown); however, expansion of proliferative crypt stem cells was reduced in *β-cat*$^{c.a.}$/*Rela*$^{\Delta IEC}$ mice when compared to *β-cat*$^{c.a.}$ mutants (Figures 2B–2E) and alkaline phosphatase staining, labeling differentiated, and absorptive enterocytes confirmed an increased villus-to-crypt cell ratio in *β-cat*$^{c.a.}$/*Rela*$^{\Delta IEC}$ mice (Figures 2F and 2G). Consistently, with a more differentiated phenotype, RelA-deficient *β-cat*$^{c.a.}$ mice retained a significantly higher expression of mRNAs encoding sucrase-isomaltase, MUC-2, and synaptophysin, which are markers for enterocytes, goblet cells, and enteroendocrine cells, respectively (Figure 2H). Furthermore, comparative gene expression analysis and gene set enrichment

(N) Quantification of nuclear RelA/p65-expressing IEC. Data are mean ± SE; n ≥ 3; ***p < 0.0001 by t test.
(O) NF-κB activity can be blocked by administration of etanercept but not anakinra. Specificity of NF-κB complex was confirmed by competition assay with 50-fold unlabeled oligonucleotide.
(P) Kaplan-Meier survival curve of *β-cat*$^{c.a.}$/*Tnf*$^{-/-}$ compound mutant mice (pink solid line; n = 9) compared to *β-cat*$^{c.a.}$/*Tnf*$^{+/-}$ mice (pink dashed line; n = 13; p < 0.0001 by log rank test). Note that survival of *β-cat*$^{c.a.}$/*Tnf*$^{+/-}$ mice was comparable to *β-cat*$^{c.a.}$ mice (dashed black line).

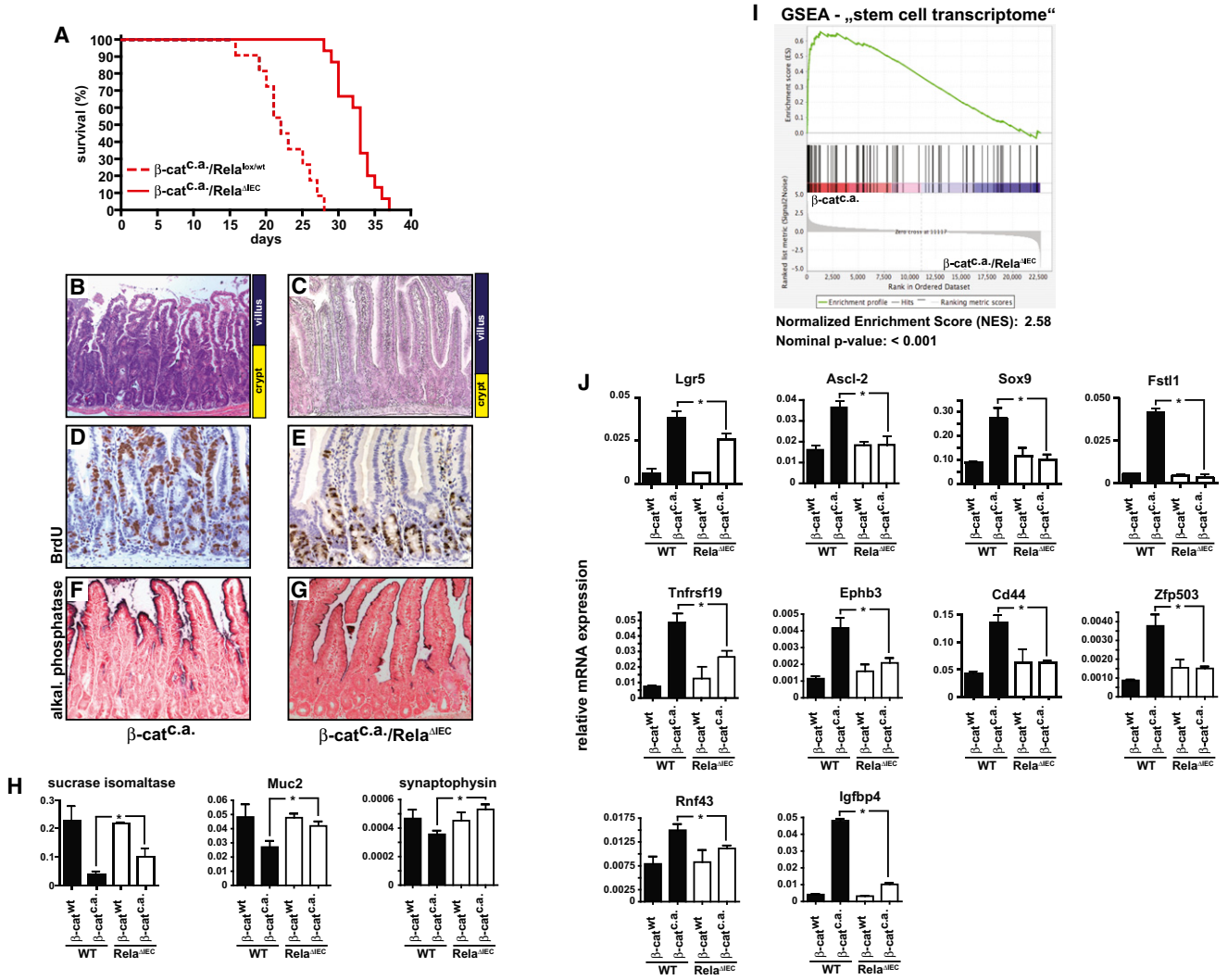

Figure 2. Loss of *Rela* in *β-cat*$^{c.a.}$ IEC Prolongs Survival and Inhibits Stem Cell Expansion

(A) Kaplan-Meier survival curve of heterozygous floxed *Rela* mice (*β-cat*$^{c.a.}$/*Rela*$^{lox/WT}$; n = 12) and *β-cat*$^{c.a.}$/*Rela*$^{\Delta IEC}$ mice (n = 13), p = 0.0001 by log rank test.

(B–E) Representative H&E stained sections (B and C) and immunohistochemical analysis (D and E) of *β-cat*$^{c.a}$ and *β-cat*$^{c.a.}$/*Rela*$^{\Delta IEC}$ mice on day 15 of the model showing reduced crypt expansion as well as decreased expression of BrdU in *β-cat*$^{c.a.}$/*Rela*$^{\Delta IEC}$ mice (C and E) compared to *β-cat*$^{c.a}$ mice (B and D; proliferation index: 0.31 ± 0.016 in *β-cat*$^{c.a}$ mice versus 0.13 ± 0.006 in *β-cat*$^{c.a.}$/*Rela*$^{\Delta IEC}$ mice; data are mean ± SE; n = 3 of each genotype; p < 0.0001).

(F and G) Alkaline phosphatase staining of small intestinal sections from *β-cat*$^{c.a.}$ and *β-cat*$^{c.a.}$/*Rela*$^{\Delta IEC}$ mice on day 15 of the model.

(H) Relative mRNA expression of differentiation markers in IEC of WT and *β-cat*$^{c.a.}$, as well as *Rela*$^{\Delta IEC}$ and *β-cat*$^{c.a.}$/*Rela*$^{\Delta IEC}$ mice on day 15. Data are mean ± SE; n ≥ 3; *p < 0.05 by t test.

(I) GSEA analysis comparing *β-cat*$^{c.a.}$ and *β-cat*$^{c.a.}$/*Rela*$^{\Delta IEC}$ probe sets with "stem cell transcripts."

(J) Relative mRNA expression of intestinal stem cell markers in IEC of WT and *β-cat*$^{c.a.}$, as well as *Rela*$^{\Delta IEC}$ and *β-cat*$^{c.a.}$/*Rela*$^{\Delta IEC}$ mice on day 15. Data are mean ± SE; n ≥ 3; *p < 0.05 by t test.

analysis (GSEA) on RNA samples isolated from IEC of wild-type, *Rela*$^{\Delta IEC}$, *β-cat*$^{c.a.}$, and *β-cat*$^{c.a.}$/*Rela*$^{\Delta IEC}$ mice 15 days after tamoxifen administration revealed a marked downregulation of a large number of Wnt targets in IEC of *β-cat*$^{c.a.}$/*Rela*$^{\Delta IEC}$ mice recently identified as components of an "intestinal stem cell transcriptome" (van der Flier et al., 2009) compared to *β-cat*$^{c.a.}$ (normalized enrichment score 2.58, p < 0.001; Figure 2I). Differential expression of several of these stem cell genes, such as *Lgr5*, *Ascl2*, *Tnfrsf19*, *Fstl1*, *Ephb3*, *Cd44*, *Rnf43*, *Igfbp4*, *Zfp503*, and *Sox9* was validated by quantitative real-time PCR (Figure 2J). Collectively, these data suggested that NF-κB could affect the development of a crypt progenitor phenotype and the initiation of adenomatous cell transformation through the regulation of Wnt-dependent intestinal stem cell gene expression.

NF-κB Directly Interacts with β-Catenin and Modulates β-Catenin Binding Activity

β-catenin can physically interact with RelA/p50 dimers in various human cancer cell lines (Deng et al., 2002). In light of the profound differential regulation of the Wnt-dependent stem cell

signature in RelaA/p65-deficient β-*cat*$^{c.a.}$ mice, we tested whether NF-κB could possibly complex with β-catenin in primary IEC as well and whether this interaction might affect β-catenin's binding to the Tcf/Lef consensus motif. Indeed, when we pulled down endogenous β-catenin from IEC of wild-type and β-*cat*$^{c.a.}$ mice, RelA/p65 was weakly bound to the immunoprecipitated protein from wild-type IEC, but this interaction was strongly enhanced upon β-catenin stabilization (Figure 3A). To assess β-catenin DNA-binding activity in IEC, we performed DNA affinity precipitation assays (DAPA) by using a biotinylated Tcf/Lef consensus sequence to precipitate proteins that bind specifically the Tcf/Lef motif. Immunoblotting of the precipitates confirmed that stabilization of mutant β-catenin strongly induced its binding to DNA, which, however, was greatly diminished in the absence of RelA/p65 and absent when a mutant control oligonucleotide was used (Figure 3B). Moreover, a direct association of RelA/p65 with the promoters of these Wnt-regulated stem cell genes was confirmed by quantitative chromatin immunoprecipitation (ChIP) assay (Figure 3C). Association of β-catenin and RelA/p65 at these promoter regions was confirmed by Re-ChIP analysis (Figure 3D). To rule out that changes in DNA binding were caused by the skewed crypt-villus ratio in mice of different genotypes, we confirmed that TNFα could increase binding of β-catenin to the Tcf/Lef motif in 293 cells that had been transfected with a S33Y mutant of β-catenin along with wild-type Tcf4 (Figure 3E). Furthermore, a constitutively active form of IKKβ (IKKβ^{EE}) also dose dependently induced interaction of β-catenin and Tcf-4, β-catenin and RelA/p65, and β-catenin and CREB-binding protein (CBP), a common coactivator of both NF-κB and β-catenin (Figure 3F) suggesting that NF-κB could modify Wnt-signaling through recruitment of CBP. Indeed, siRNA mediated CBP knockdown confirmed that β-catenin/p65 interaction and TNFα-induced increase in Wnt-reporter activity was dependent on the presence of this coactivator (Figures 3G and 3H).

Loss of *Ikba* Accelerates Crypt Transformation and Suggests Dedifferentiation of IEC in β-*cat*$^{c.a.}$ Mice

To examine whether enhanced NF-κB activation could conversely promote crypt stem cell expansion, we crossed β-*cat*$^{c.a.}$ mice to floxed *Ikba* mice (Rupec et al., 2005), enabling IEC-specific constitutive NF-κB activity along with persistent β-catenin/Tcf4 signaling in β-*cat*$^{c.a.}$/*Ikba*$^{\Delta IEC}$ compound mutants. Expectedly, deletion of IκBα enhanced NF-κB binding in IEC (Figure 4A) and accelerated IEC transformation, leading to a significantly shortened survival of β-*cat*$^{c.a.}$ mice by 32% (median survival was 22 days in β-*cat*$^{c.a.}$/*Ikba*$^{lox/WT}$ versus 15 days in β-*cat*$^{c.a.}$/*Ikba*$^{\Delta IEC}$ mice; Figure 4B). Pronounced NF-κB activation increased β-catenin binding and recruitment of RelA/p65 to the Tcf/Lef consensus site and enhanced interaction of β-catenin with CBP (Figure 4C) further demonstrating that NF-κB can recruit CBP to interact with β-catenin thus stimulating Wnt-dependent transcription. Apart from a massive accumulation of highly proliferative, crypt stem cells expressing c-*myc* (data not shown), β-*cat*$^{c.a.}$/*Ikba*$^{\Delta IEC}$ double mutants frequently displayed aberrant foci along the villus epithelium resembling crypt structures (Figure 4D). These foci were actively proliferating and expressed nuclear β-catenin as well as the crypt marker c-*myc* (Figures 4E–4G) and could be detected within 24 hr after tamoxifen administration (Figure S1 available online). Furthermore, in situ proximity ligation assay confirmed direct interaction of RelA/p65 and β-catenin in these cells (Figure 4H). Previous reports had demonstrated that *Apc*-deficient crypt cells fail to migrate out of the crypt due to maintenance of EphB expression, which results in subepithelial transformed clones (Batlle et al., 2002). Similarly, crypt-like foci in β-*cat*$^{c.a.}$/*Ikbα*$^{\Delta IEC}$ mice expressed EphB3 (Figure 4I) and detached from the surrounding villus epithelium and invaded into the subepithelium, where they formed adenomatous crypts (Figure S1). However, these results seemed to be in apparent contrast to the notion that intestinal cancers arise from Lgr-5-positive *crypt* stem cells rather than postmitotic *differentiated* enterocytes (Barker et al., 2009). We therefore asked whether the observed villus crypt-like foci could have regained stem cell properties, formally enabling them to initiate formation of adenomatous crypts. Indeed, *Ikba*-deficient villus crypt-like foci expressed Ascl-2 and SOX9 (Figures 4J and 4K) as well as the stem cell markers *Lgr5* and *Rnf43* (Figures 4L and 4M). These data suggested that NF-κB mediated enhancement of β-catenin signaling in villus cells allowed a dedifferentiation program and occurrence of crypt stem cells in an aberrant position. Re-expression of the stem cell marker Lgr5 in these newly formed crypts supported the hypothesis that these cells could initiate adenomatous crypt formation. Interestingly, however, loss of IEC IκBα alone was not sufficient to enhance transcription of crypt stem cell markers in β-catenin wild-type mice (Figure S1).

Villus Cells Can Dedifferentiate Ex Vivo and Form Spheroids that Have the Capacity to Form Tumors

To confirm that villus cells have the capacity to dedifferentiate and to regain stem cell properties when β-catenin signaling is hyperactivated, we employed a recently developed organoid culture system (Sato et al., 2009) by using IEC from *villin-cre*ER^{T2}/*Apc*$^{lox/lox}$ (*Apc*$^{\Delta IEC}$) or *villin-cre*ER^{T2}/*Apc*$^{lox/lox}$/*K-ras*$^{G12D/+}$ mice (*Apc*$^{\Delta IEC}$/*K-ras*^{G12D}) mice. Oncogenic K-ras strongly cooperates with deregulated Wnt signaling conferred by *Apc* loss or activating *Ctnnb* mutations (Bennecke et al., 2010; Janssen et al., 2006; Sansom et al., 2006), although it can also induce NF-κB activation (Perkins, 2012). In contrast to wild-type crypts that maintained dependence on the presence of R-spondin in the culture medium, cultured crypts derived from both *Apc*$^{\Delta IEC}$ and *Apc*$^{\Delta IEC}$/*K-ras*^{G12D} formed spheroids, histologically resembling adenomas, even in the absence of R-spondin because of constitutively active Wnt signaling when crypts were isolated 2 days after a single tamoxifen administration (Figures 5A and 5B). *Apc*$^{\Delta IEC}$/*K-ras*^{G12D} crypt cells were characterized by markedly elevated NF-κB activation compared to cells from *Apc* single mutants (Figure 5C). Next, we examined whether villi isolated from *Apc*$^{\Delta IEC}$ and *Apc*$^{\Delta IEC}$/*K-ras*^{G12D} mice would convert into R-spondin-independent spheroids when isolated 2 days after tamoxifen administration. At this time point villi of mice of both genotypes appeared histologically comparable and did not contain any Lgr5^{+} cells (Figure S2). Although villi from wild-type or *Apc*$^{\Delta IEC}$ mice did not survive in culture, villi isolated from *Apc*$^{\Delta IEC}$/*K-ras*^{G12D} compound mutants formed spheroid structures that could indeed be maintained without

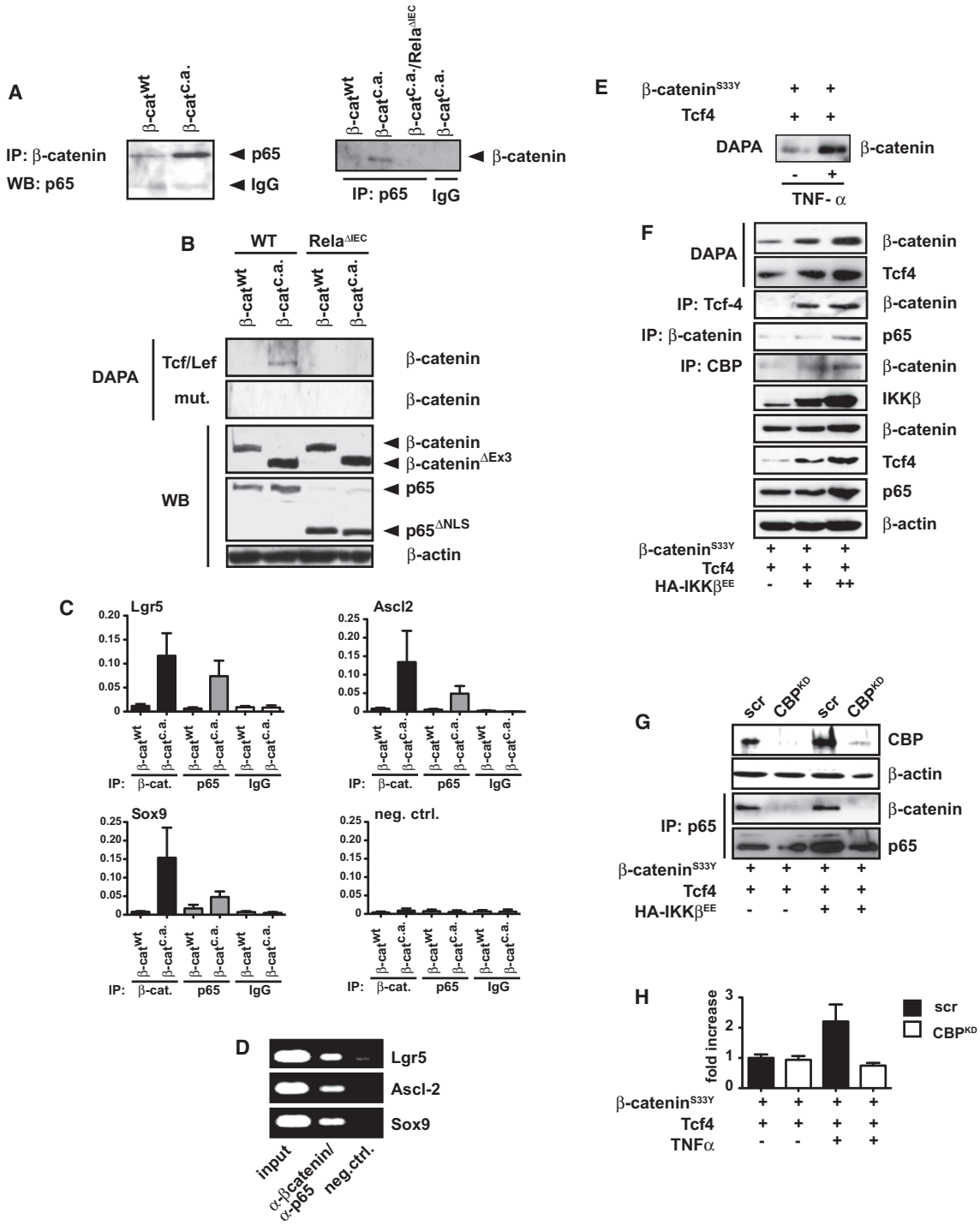

Figure 3. NF-κB and β-Catenin Interact via CBP to Modulate β-Catenin DNA Binding

(A) Immunoblot analysis of proteins that were immunoprecipitated from lysates from WT and *β-cat*$^{c.a.}$ mice on day 15.

(B) DNA affinity precipitation assay (DAPA) and immunoblot analysis (WB) of lysates prepared from isolated IEC from WT and *β-cat*$^{c.a.}$, as well as *Rela*$^{\Delta IEC}$ and *β-cat*$^{c.a.}$*/Rela*$^{\Delta IEC}$ mice on day 15.

(C) Quantitative chromatin immunoprecipitation (ChIP) assay on DNA isolated from IEC of WT and *β-cat*$^{c.a.}$ mice on day 15. Precipitated DNA or 10% of chromatin input was amplified with gene-specific primers amplifying promoter regions, which contain β-catenin/Tcf consensus motifs (Yochum et al., 2007) but no classical κB-binding sites. Data are mean ± SE; n ≥ 4.

(D) Re-ChIP assay on DNA isolated from IEC of a *β-cat*$^{c.a.}$ mouse on day 15 with a β-catenin antibody for the first precipitation followed by a second immunoprecipitation after DNA isolation with p65 antibody. In negative control second immunoprecipitation was omitted.

(legend continued on next page)

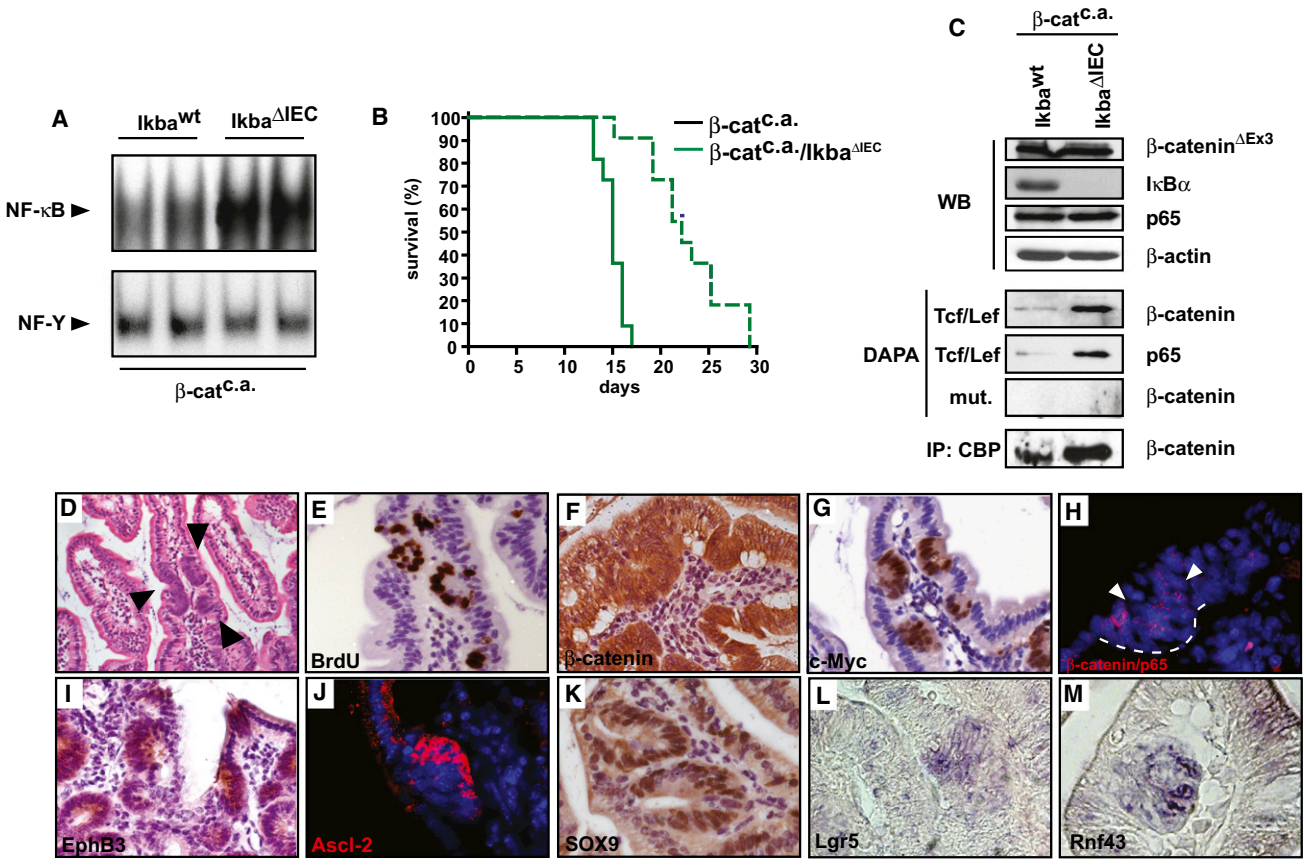

Figure 4. Increased NF-κB Activity Shortens Survival and Induces Dedifferentiation of Villus Cells in *β-cat*$^{c.a.}$ Mice

(A) NF-κB binding activity in IEC isolated from *Ikba*-deficient *β-cat*$^{c.a.}$ mice on day 10.

(B) Kaplan-Meier survival curve of *β-cat*$^{c.a.}$/*Ikba*$^{\Delta IEC}$ mice (n = 11) and *β-cat*$^{c.a.}$ *Ikba*$^{lox/WT}$ mice (n = 12); $p < 0.0001$ by log rank test.

(C) Immunoblot analysis (WB) and DAPA of lysates prepared from isolated IEC from *β-cat*$^{c.a}$ and *β-cat*$^{c.a.}$/*Ikba* $^{\Delta IEC}$ mice on day 10.

(D) Representative H&E stained section of a *β-cat*$^{c.a.}$/*Ikba*$^{\Delta IEC}$ villus on day 10. The arrowheads indicate crypt-like cell structures in an aberrant localization.

(E–G) Immunohistochemical analysis of *β-cat*$^{c.a.}$/*Ikba*$^{\Delta IEC}$ villus crypt-like structures.

(H) Duolink proximity ligation assay demonstrating close proximity of β-catenin and RelA/p65 suggesting interaction in *β-cat*$^{c.a.}$/*Ikba*$^{\Delta IEC}$ villus crypt-like structures. Dashed white line marks aberrant crypt structure, arrowheads denote regions of signal amplification (red). Nuclei are stained with DAPI.

(I–K) Aberrant villus crypts express stem cell markers EphB3 (I), ASCL-2 (J) and SOX9 (K).

(L and M) In situ hybridization with probes specific for *Lgr5* and *Rnf43* reveals stem cell properties of *β-cat*$^{c.a.}$/*Ikba*$^{\Delta IEC}$ villus crypt-like structures.

See also Figure S1.

R-spondin (Figure 5D). Similar results could be obtained with villus cells derived from *β-cat*$^{c.a.}$/*Ikbα*$^{\Delta IEC}$ mice (data not shown). Importantly, the specific IKKβ inhibitor ML120B (Nagashima et al., 2006) completely abolished spheroid formation in *Apc*$^{\Delta IEC}$/*K-ras*^{G12D} villus cells and reduced sphere formation of *Apc*$^{\Delta IEC}$/*K-ras*^{G12D} crypts by more than 60% (Figures 5D and 5E). Spheroids originating from *Apc*$^{\Delta IEC}$/*K-ras*^{G12D} villus or crypt cells were morphologically comparable (Figures 5F–5I) and both retained their size over several passages (Figure 5J), supporting the notion that they both comprised cancer stem cells. Indeed, when we injected *Apc*$^{\Delta IEC}$/*K-ras*^{G12D} villus-derived spheroids subcutaneously into nude mice, they formed tumors with growth characteristics similar to those of the crypt-derived spheroids (Figure 5K). Tumors from both crypt and villus-derived spheres were highly proliferative, strongly expressed Lgr5 (Figure 5L), and developed independently of spheroid passage number (Figure S2). Lysozyme^{+} Paneth cells were detectable in tumors of either origin (Figure 5L), further underscoring the pluripotent potential of spheroids derived from both crypts and villi. When we separated Lgr5^{+} and Lgr5^{-} cells from villus-derived spheres,

(E and F) DNA affinity precipitation assay (DAPA, [E]), and immunoblot analysis (WB) (F) of protein lysates prepared from 293 cells transfected with β-catenin^{S33Y} and Tcf-4, that were either stimulated with TNF-α (10 ng/ml) for 60 min (E) or cotransfected with increasing amounts (0, 0.5, and 1 μg) of IKKβ^{EE} (F).

(G) Immunoblot analysis of protein lysates prepared from 293 cells transfected with β-catenin^{S33Y} and Tcf-4 along with scramble siRNA control or a CBP targeting siRNA pool.

(H) Relative luciferase activity with a Tcf/Lef reporter (TOPFLASH) in protein lysates prepared from 293 cells transfected with β-catenin^{S33Y} and Tcf-4 along with scramble siRNA control or a CBP targeting siRNA pool untreated or stimulated with TNF-α (10 ng/ml) for 8 hr. Data are mean ± SE; $n \geq 3$.

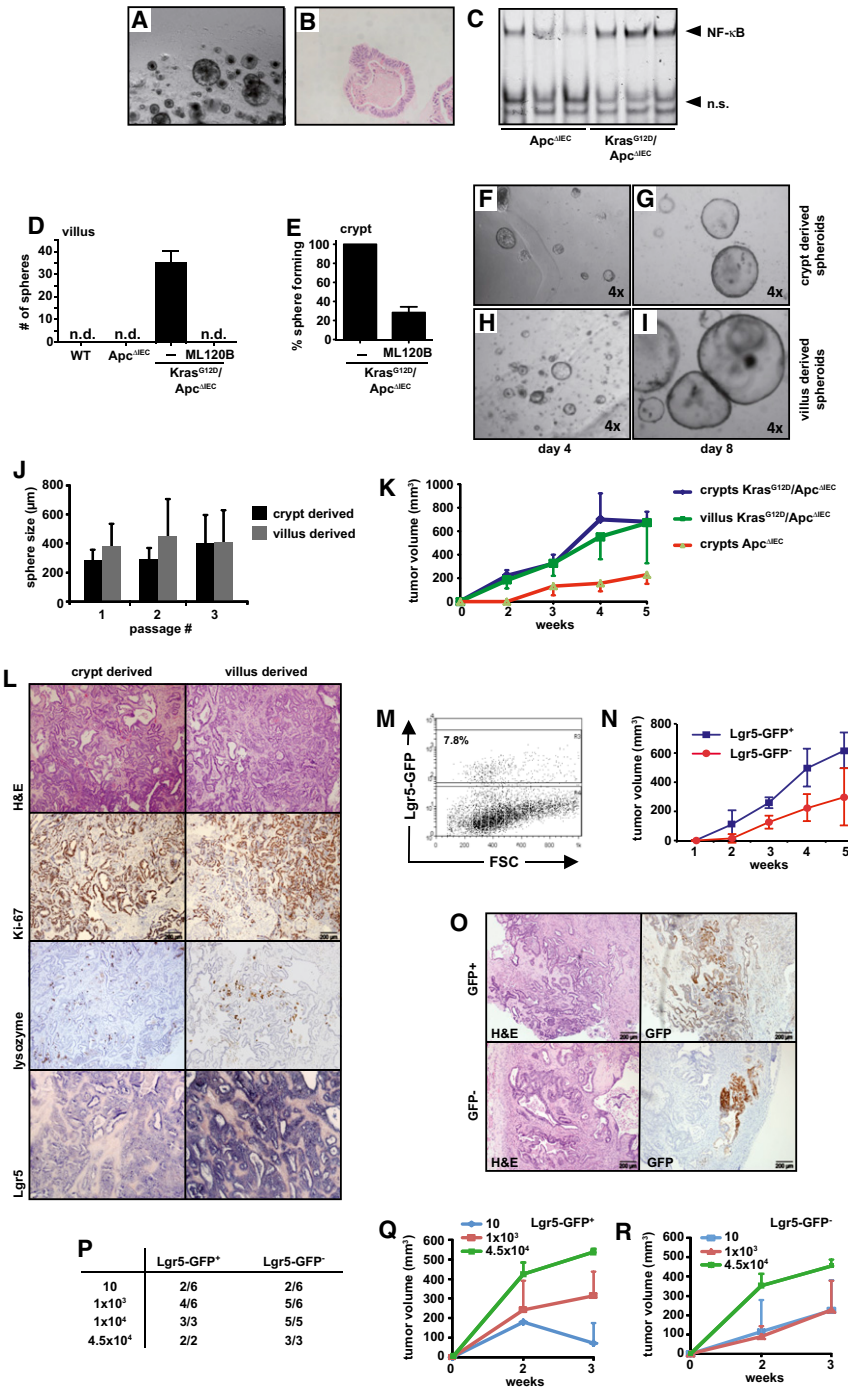

Figure 5. Oncogenic K-ras Cooperates with Wnt Signaling to Dedifferentiate Villus Cells into Intestinal Tumor Stem Cells in a NF-κB Dependent Manner

(A and B) Morphology of R-spondin-independent spheroids generated of crypts from *Apc*$^{\Delta IEC}$ mice.

(C) Elevated NF-κB activity in crypts from *Apc*$^{\Delta IEC}$/*K-ras*^{G12D} compared to *Apc*$^{\Delta IEC}$ mice.

(D) Quantification of R-spondin-independent spheroids derived from villi of mice of indicated genotypes in the presence or without the specific IKKβ inhibitor ML120B (n = 5/genotype; n.d.: not detectable).

(E) Inhibition of crypt-derived spheroids by ML120B.

(F–I) Morphology of crypt or villus-derived spheroids from *Apc*$^{\Delta IEC}$/*K-ras*^{G12D} mice after 4 (F and H) and 8 days (G and I) in culture.

(J) Sphere formation assay comparing crypt and villus-derived spheres derived from *Apc*$^{\Delta IEC}$/*K-ras*^{G12D} mice. Data are mean ± SE; n ≥ 3.

(K) Tumor growth in CD1 athymic mice after subcutaneous injection of crypt or villus-derived spheroids originating from mice of indicated genotypes. Data are mean ± SE; n ≥ 3.

(L) Comparative histological analysis of a representative tumor grown in CD1 athymic mice 22 days after the subcutaneous injection of spheroids originating from *Apc*$^{\Delta IEC}$/*K-ras*^{G12D} crypts or villi. Lgr5 expression was detected by in situ hybridization.

(M) FACS plot of villus-derived spheroids from an *Apc*$^{\Delta IEC}$/*K-ras*^{G12D}/*Lgr5-EGFP-IRES-cre*ER^{T2} compound mutant. Absence of Lgr5 in the GFP$^-$ population was confirmed by PCR (data not shown).

(N) Tumor growth in CD1 athymic mice after subcutaneous injection of equal number of Lgr5$^+$ or Lgr5$^-$ cells from villus-derived spheroids plotted in (M). Data are mean ± SE; n ≥ 3.

(O) Immunohistochemical analysis of EGFP indicating expression of Lgr5 in tumors originating from Lgr5$^+$ or Lgr5$^-$ villus cells.

(P) Incidence of subcutaneous tumor growth in CD1 athymic mice after injection of 10, 1 × 10^3, 1 × 10^4 or 4.5 × 10^4 GFP$^+$ (indicating Lgr5$^+$) or GFP$^-$ (indicating Lgr5$^-$) cells from villus-derived spheroids.

(Q and R) Tumor growth kinetics in CD1 athymic mice after subcutaneous injection of indicated number of Lgr5$^+$ (Q) or Lgr5$^-$ cells (R) from villus-derived spheroids. Data are mean ± SE. See also Figure S2.

both populations retained the capacity to initiate subcutaneous tumor growth with similar kinetics (Figures 5M and 5N) even when we performed serial transplantations over several passages (data not shown), and tumors from initially Lgr5$^-$ population re-expressed Lgr5 (Figure 5O). Moreover, limiting dilution experiments did not reveal any differences in the ability to initiate subcutaneous tumors between Lgr5$^+$ and Lgr5$^-$ cells from villus-derived spheres (Figures 5P–5R). Collectively, these results strongly support the notion that villus cells can reacquire cancer stem cell properties by dedifferentiation when Wnt signaling is elevated in a NF-κB-dependent manner.

Hyperactivation of β-Catenin Signaling in Lgr5$^-$ Cells Induces Dedifferentiation and Initiation of Tumorigenesis

Because *villin-cre*ER^{T2} mice recombine in both Lgr5$^-$ differentiated and Lgr5$^+$ stem cells, crypt-like foci in *β-cat*$^{c.a.}$ and *β-cat*$^{c.a.}$/*Ikbα*$^{\Delta IEC}$ mice could theoretically have originated from the

Lgr5$^+$ cells at the base of the crypt and migrated upward. Thus, in order to formally prove that dedifferentiated villus cells can initiate tumorigenesis in vivo, we generated a Cre-expressing mouse that allowed recombination in Lgr5$^-$ cells only. Based on the observation that splicing and thus activation of the transcription factor X-box-binding protein 1 (XBP1), a key component of the endoplasmatic reticulum (ER) stress response, constitutively occurs under physiologic unchallenged conditions in Lgr5$^-$ IEC, but not Lgr5$^+$, stem cells (J.H. and G.R.v.d.B., unpublished data, and Figure S3), we hypothesized that *Xbp1s-cre*ER^{T2} mice would permit recombination specifically in Lgr5$^-$ IEC. Indeed, lack of recombination in Lgr5$^+$ and Bmi1$^+$ stem cells was confirmed by lineage tracing in *Xbp1s-cre*ER^{T2}-*Rosa26R-dtTomato* mice (Figures 6A–6C). Within 24 hr, red fluorescence indicating recombination was detectable in IEC above the crypt villus junction as well as in Paneth cells, a cell type in which XBP splicing confers important functions (Kaser et al., 2008) (Figures 6A and 6B). Importantly, PCR on FACS-sorted RFP-positive and -negative IEC confirmed absence of Lgr5$^+$ or Bmi1$^+$ expression in RFP$^+$ cells. Consequently, 33 days after tamoxifen administration, red fluorescent IEC were completely absent. Lack of recombination by Xbp1s-Cre in Lgr5$^+$ or Bmi1$^+$ stem cells was further functionally confirmed and considered the missing adenomatous transformation or stem cell expansion in mice with single activation of β-catenin only in Lgr5$^-$ IEC of *Xbp1s-cre*ER^{T2}/*Ctnnb*$^{loxEx3/WT}$ compound mutants (Figures 6E–6G). In contrast, loss of a *Ctnnb* exon 3 in Lgr5$^+$ stem cells using *Lgr5-EGFP-IRES-cre*ER^{T2}/*Ctnnb*$^{loxEx3/WT}$ mice resulted in massive transformation and death of the animals within 45 days (Figure 6E) similar to the results of previously reported *Bmi1-cre*ER^{T2}/*Ctnnb*$^{loxEx3/WT}$ mice (Sangiorgi and Capecchi, 2008). However, when β-catenin activation was enhanced by the concomitant loss of IκBα in homozygous *Xbp1s-cre*ER^{T2}/*Ctnnb*$^{loxEx3/loxEx3}$/*Iκbα*$^{lox/lox}$ mice or the simultaneous activation of oncogenic K-ras in *Xbp1s-cre*ER^{T2}/*Ctnnb*^{loxEx3}/*Kras*^{G12D} compound mutants, tumor initiation commenced and adenomatous polyps occurred within 30 days (Figures 6H and 6J), recapitulating the phenotype we had observed in the organoid culture system. These polyps were highly proliferative and characterized by elevated NF-κB activation when compared to IEC of *β-cat*$^{c.a.}$ mice (Figure S3). Most importantly tumors re-expressed stem cell markers Lgr5 and Rnf43 (Figures 6H and 6J) and displayed increased expression of genes encoding members of the "stem cell signature" (Figure 6I) providing direct genetic evidence for dedifferentiation of Lgr5$^-$ IEC in vivo. In agreement with the lineage tracing data (Figure 6A), expression of nuclear β-catenin and Ki-67 could be observed in cells above the crypt-villus junction 24 hr after tamoxifen administration in mice (Figures 6K and 6L), suggesting that these comprised the cells of origin of tumors in *Xbp1s-cre*ER^{T2}/ *Ctnnb*^{loxEx3}/*Kras*^{G12D} mice.

DISCUSSION

Cell-type plasticity as it can be observed during epithelial-mesenchymal transition (EMT) has been suggested to be an important prerequisite for the metastatic spread of solid tumors during the tumor progression stage (Polyak and Weinberg, 2009). EMT correlates with β-catenin expression in colorectal cancer and has been associated with dedifferentiation of invading cells (Brabletz et al., 2005). Accordingly, it was recently suggested that dedifferentiation of nonstem cells triggered by signals from the inflammatory microenvironment may also lead to the generation of cancer stem cells (Gupta et al., 2009; Hanahan and Weinberg, 2011). So far, in vivo evidence for the existence of dedifferentiation has been limited to mouse differentiating spermatogonia that can generate germinal stem cells (Barroca et al., 2009) as well as mammary luminal cells that can convert into mammary stem cells upon overexpression of Sox9 and Slug (Guo et al., 2012). In the context of tumorigenesis a subpopulation of basal-like human mammary epithelial cells recently was shown to spontaneously convert into cancer-stem-cell-like cells in vitro (Chaffer et al., 2011). Here, we demonstrate in a genetic model of intestinal tumor initiation that epithelial nonstem cells can re-express stem cell markers and can be converted into tumor-initiating cells. This phenomenon is strictly dependent on the degree of Wnt activation and can only be observed when Wnt signaling is markedly elevated. Two models for the histopathogenesis of colorectal cancer have been proposed: a "top-down" model suggesting that dysplastic cells spread laterally and downward to form new crypts (Shih et al., 2001) and a "bottom-up" model that is based on transformation and expansion of crypt stem cells (Preston et al., 2003). Recently, it was demonstrated that Lgr5$^+$ cells comprise the tumor-initiating cell population (Barker et al., 2009), whereas they can be repopulated by Bmi1$^+$ cells after tissue damage (Tian et al., 2011). Because under physiological circumstances these cells reside exclusively at the bottom of intestinal crypts (Barker et al., 2007), the "bottom-up" model seemed to represent the prevailing concept. We now provide genetic evidence that Lgr5$^-$ enterocytes have the potential to dedifferentiate and to reacquire stem cell properties including Lgr5 expression lending support for a "top-down" model. Thus, we suggest that these models do not exclude each other and that tumor-initiating mutations can occur in both Lgr5$^+$ crypt stem cells or in more differentiated Lgr5$^-$ cells, as long as these initially negative cells dedifferentiate and re-express Lgr5 (Figure 7).

Reprogramming of differentiated cells into induced pluripotent cells (iPS) ex vivo can be achieved through the combined activation of selective transcription factors (Jaenisch and Young, 2008). Thus, it is reasonable that IEC also may have the capacity to dedifferentiate in vivo as long as the required transcriptional program for such process, in this case Wnt signaling, is strongly enough activated. Our results agree with previous findings and show that neither in vitro nor in vivo single stabilization of β-catenin nor loss of *Apc* alone is sufficient to drive dedifferentiation (Barker et al., 2009). However, concomitant activation of cooperating oncogenes, such as K-ras, as well as cytokine-triggered activation of NF-κB enhances β-catenin/Tcf-mediated transcriptional activity that provides initial nonstem cell IEC with tumor stem cell properties. This may suggest that induction of a single pathway may be sufficient to induce dedifferentiation toward a tissue-specific stem cell compared to the activation of several factors required for pluripotency (Jaenisch and Young, 2008). However, we cannot entirely rule out additional direct

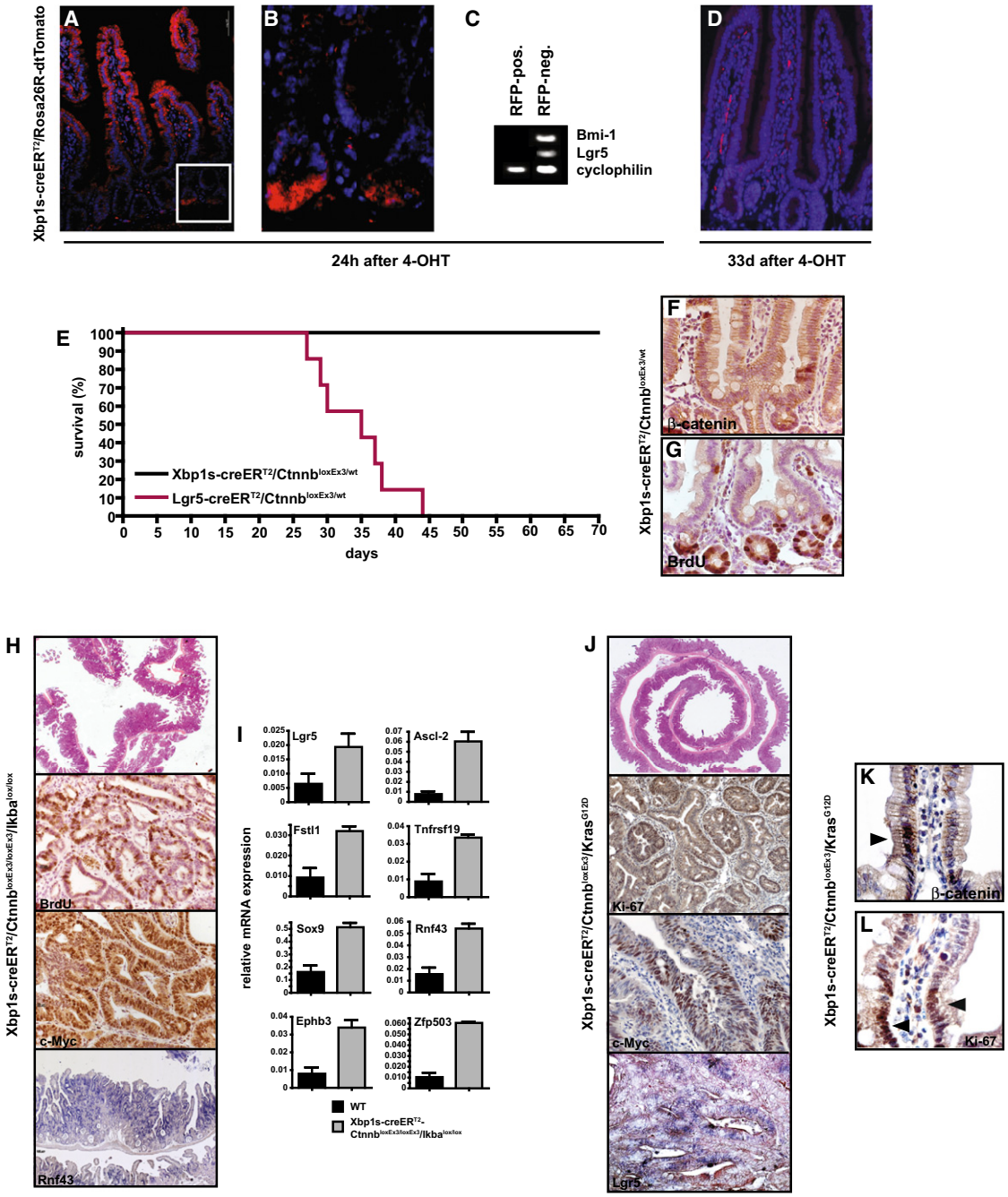

Figure 6. Dedifferentiation of Nonstem Cells Allows Initiation of Tumorigenesis In Vivo

(A and B) RFP expression in *Xbp1s-cre*ER^{T2}-*Rosa26R-dtTomato* mice 24 hr after tamoxifen administration indicating recombination in cells above the crypt villus junction (A) and in Paneth cells (B).

(C) PCR indicates expression of stem cell markers Lgr5 and Bmi1 only in nonrecombined RFP^{-} stem cells.

(D) Absence of RFP expression in IEC of *Xbp1s-cre*ER^{T2}-*Rosa26R-dtTomato* mice 33 days after tamoxifen administration.

(E) Kaplan-Meier survival curve of *Lgr5-IRES-EGFP-cre*ER^{T2}/*Ctnnb*$^{loxEx3/WT}$ (n = 7) and *Xbp1s-cre*ER^{T2}/*Ctnnb*$^{loxEx3/WT}$ (n = 8) mice that were given the same amount of tamoxifen (5 × 1 mg), $p < 0.0001$ by log rank test. Note that differences in survival between *β-cat*$^{c.a.}$ *mice* (Figure 1A; *villin-cre*ER^{T2}/*Ctnnb*$^{loxEx3/WT}$) and *Lgr5-IRES-EGFP-cre*ER^{T2}/*Ctnnb*$^{loxEx3/WT}$ mice is due to a lower recombination efficiency in *Lgr5-IRES-EGFP-cre*ER^{T2} mice causing a lower frequency of actual stem cell hits (P.C. and O.J.S. et al., unpublished data).

(F and G) Immunohistochemical staining of β-catenin (F) and BrdU (G) in intestines of *Xbp1s-cre*ER^{T2}/*Ctnnb*$^{loxEx3/WT}$ mice 50 days after the first tamoxifen administration confirms only sporadic positively stained cells outside the crypt compartment.

(H) Representative H&E staining, immunohistochemical analysis of BrdU incorporation and c-*myc* as well as in situ hybridization of *Rnf43* in the proximal small intestine from a *Xbp1s-cre*ER^{T2}/*Ctnnb*$^{loxEx3/loxEx3}$/*Ikbα*$^{lox/lox}$ mouse 29 days after tamoxifen administration confirming re-expression of stem cell markers.

(legend continued on next page)

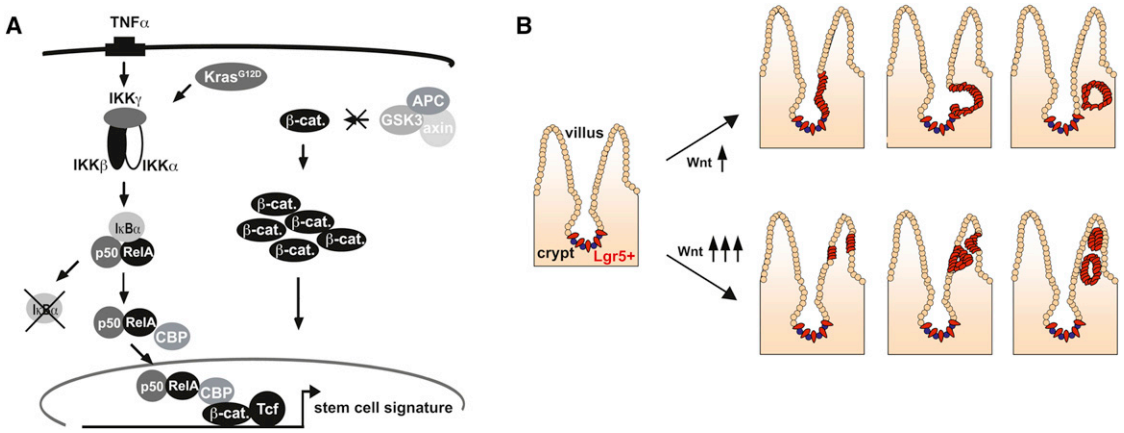

Figure 7. "Bottom-Up" and "Top-Down" Models of Intestinal Tumorigenesis Do Not Exclude Each Other

(A) Model summarizing the proposed signaling mechanism in IEC: TNFα or oncogenic K-ras enhance β-catenin activation through induction of canonical NF-κB activation, which leads to recruitment of CBP and binding to β-catenin/Tcf to enhance transcription of Wnt-dependent stem cell genes.

(B) Schematic presentation of two possible ways of polyp formation that depend on the extent of Wnt activation: in case of modest Wnt activation caused by loss of *Apc* or *Ctnnb* mutation stem cell expansion and tumorigenesis is initiated only when $Lgr5^+$ crypt stem cells (red) are mutated otherwise cells are shed off. Mutated $Lgr5^+$ cell invaginate around the crypt villus junction and invade into the subepithelium representing the "bottom-up" model. The lower model suggests that initially $Lgr5^-$ cells reacquire Lgr5-expression upon enforced β-catenin signaling, therefore providing these dedifferentiated cells with the same properties as crypt stem cells (i.e., Lgr5 expression) to invade into the subepithelium thus providing evidence that the top-down model and the bottom-up model of adenoma morphogenesis do not exclude each other.

See also Figure S4.

effects of K-ras and NF-κB on some of the essential stem cell genes considering that NF-κB has recently been reported to control expression of Ascl-2 (Vlantis et al., 2011).

Various modes of cross-regulation between NF-κB and β-catenin signaling pathways have been proposed in different tumor cell lines (Deng et al., 2002; Spiegelman et al., 2000). We propose that in primary IEC, NF-κB enhances Wnt-signaling by binding of RelA/p65 to β-catenin via CBP. Although it was suggested that β-catenin activation inhibits NF-κB in colon cancer cells (Deng et al., 2002), we show that stabilization of mutant β-catenin is associated with elevated NF-κB activation in primary IEC in vivo. This is at least in part dependent on TNFα that acts in a paracrine or presumably autocrine manner because most TNFα in intestine originates from IEC (Chen et al., 2003; Guma et al., 2011). Interestingly, not only TNFα but also oncogenic K-ras can induce NF-κB activation in IEC, and both enhance thereby interaction of β-catenin and CBP (Figure 7 and Figure S4). Accordingly, the capacity of oncogenic K-ras to dedifferentiate *Apc*-deficient villus cells in vitro depends on NF-κB activation.

Cell-type plasticity during tumor development such as transdifferentiation has also been suggested in other tumor entities including pancreatic cancer (Gidekel Friedlander et al., 2009; Guerra et al., 2007; Wagner et al., 2001). Interestingly, during pancreatic carcinogenesis this frequently occurs in the context of tissue inflammation and allows tumor initiation from otherwise refractory cell types (Gidekel Friedlander et al., 2009; Guerra et al., 2011; Guerra et al., 2007). Similarly, in ulcerative colitis patients we found massive expansion of *OLFM4*-expressing epithelial cells in aberrant positions (Figure S4). In the absence of oncogenic mutations this may represent a physiological wound healing response and may allow de novo crypt formation thereby providing an attractive possible explanation how large ulcerations can be reconstituted in addition to crypt fission. However, at the same time this suggests that chronic inflammation may increase the number of potentially tumor-initiating cells by dedifferentiation thus providing an additional explanation of why such patients have an elevated risk of developing colon cancer. However, our data may not only be relevant for tumor initiation in the context of chronic inflammation but could also have an impact for the therapy of advanced cancers such as strategies aiming at the eradication of tumor stem cells. Particularly in colorectal tumors harboring both *APC* and *KRAS* mutations we speculate that tumor stem cells could easily be replenished by dedifferentiation. However, inhibition of IKKβ/NF-κB may be a potent strategy to prevent such effects.

In summary, we provide direct genetic evidence that dedifferentiation can lead to the formation of tumor-initiating cells that

(I) Relative mRNA expression of intestinal stem cell markers in IEC of WT and *Xbp1s-cre*ER^{T2}/*Ctnnb*$^{loxEx3/loxEx3}$/*Iκbα*$^{lox/lox}$ mice 29 days after first tamoxifen application. Data are mean ± SE; n ≥ 3.

(J) Representative H&E staining, immunohistochemical analysis of Ki-67 and c-*myc* as well as in situ hybridization of *Lgr5* in the proximal small intestine from a *Xbp1s-cre*ER^{T2}/*Ctnnb*^{loxEx3}/*K-ras*^{G12D} mouse 29 days after tamoxifen administration.

(K and L) Immunohistochemical staining of β-catenin (K) and Ki-67 (L) in mice 24 hr after tamoxifen administration indicating recombination in cells above the crypt-villus junction.

See also Figure S3.

questions a strict unidirectional model of the stem-differentiation hierarchy but rather lends support to a model of bidirectional interconvertibility (Gupta et al., 2009).

EXPERIMENTAL PROCEDURES

Mice

To delete exon 3 of *Ctnnb* in IEC, we crossed *Ctnnb*$^{loxEx3/WT}$ (Harada et al., 1999) with *villin-cre*ER^{T2} mice (kindly provided by S. Robine), *Lgr5-EGFP-IRES-cre*ER^{T2} (Barker et al., 2007), or *Xbp1s-cre*ER^{T2} mice. To delete *Apc* and to activate oncogenic K-Ras in IEC, we crossed mice carrying the conditional *Apc*^{580S} allele (Shibata et al., 1997) or *LSL-K-ras*^{G12D} (Jackson et al., 2001) with *villin-cre*ER^{T2} mice. *Xbp1s-cre*ER^{T2} transgenic mice were generated by replacing the venus coding sequence in the pCAX-F-XBP1ΔDBD-venus plasmid (Iwawaki et al., 2004) with the sequence encoding *cre*ER^{T2}. *Tnf*$^{-/-}$ and *Rosa26R-tdTomato* reporter mice were purchased from the Jackson Laboratories. All mice were on a mixed C57BL/6 × 129Sv x FVB background, and in all experiments littermate controls were used. Cre-recombinase was induced by five daily oral administrations of 1 mg tamoxifen (Sigma) in an ethanol/sunflower oil mixture. All experiments were performed under the UK Home Office guidelines as well as reviewed and approved by the Regierung von Oberbayern.

Villus Isolation and Propagation

Small intestines were washed with PBS and opened longitudinally. Villi were removed with a glass coverslip, washed in PBS, and centrifuged at 100 *g* for 3 min to separate villi from single cells. One hundred to 150 villi, mixed with 50 μl of Matrigel (BD Bioscence), were plated in 24-well plates and cultured as described (Sato et al., 2009). For transplantation experiments, 50 spheres (containing around 100 cells/sphere) were suspended in 100 μl Matrigel and injected s.c. into 6-week-old female athymic (CD1) mice.

Protein Analysis

Isolation of enterocytes, immunoblot analysis, immunecomplex kinase assay, and electrophoretic mobility shift assay (EMSA) were performed as described previously (Greten et al., 2004). In DAPA protein lysates were incubated with 2 μg of 5′ biotin labeled double-stranded oligonucleotides containing two Tcf/Lef binding sites (5′-CCCTTTGATCTTACCCCCTTTGATCTTACC-3′) or a scrambled control oligonucleotide (5′-TTTCCCCTTGATACCTTTCCCCTTGATACC-3′) in the presence of excess herring sperm DNA for 90 min at room temperature (RT) prior to pull down with Streptavidin-agarose beads (Pierce). The following antibodies were used in immunoblot analysis: α-β-catenin (Santa Cruz, SC-1496), α-RelA/p65 (SC-372), α-IκBα (SC-371), α-CBP (SC-369), α-IKKβ (Upstate 05-535), α-IKKα (IMG-136A), and α-β-actin (A4700, Sigma).

Histological Procedures and In Situ Hybridization

For alkaline phosphatase staining paraffin sections (3.5μm) were incubated for 2 hr at RT in nitroblue tetrazolium/5-bromo-4-chloro-3-indolyl phosphate solution. Nuclei were counterstained with Nuclear Fast Red (Vector). Standard immunohistochemical procedures were performed with following antibodies: α-p65 (Neo-Markers, RB-1638), α-c-*myc* (SC-788), α-β−catenin (SC-1496), α-BrdU (Amersham Bioscience RPN201), α-EphB3 (R&D Systems, AF432), α-ASCL-2 (Aviva Systems Biology, QC6671), α-SOX-9 (Chemicon Millipore, AB 5535). To detect protein interaction on paraffin sections, a Duolink Proximity Ligation Assay in situ kit (Olink Bioscience) was used according to the manufacturer's instructions and in situ hybridization was essentially performed as described previously (Barker et al., 2007).

Chromatin Immunoprecipitation Analysis

ChIP assays were performed with antibodies against β-catenin, RelA/p65, and EGFR (negative control) according to published procedures (Saccani et al., 2003). In brief, IEC were crosslinked with 1% formaldehyde for 10 min at room temperature and quenched by adding glycine (0.125 M final concentration). IEC were homogenized in lysis buffer and chromatin was fragmented by sonication. Lysates were precleared with salmon sperm/protein A agarose (Upstate) for 1 hr. Chromatin IP was performed overnight with 1.5 μg of antibody and protein G magnetic beads (Active Motif). Precipitates were washed and eluted in TE containing 2% SDS. Crosslinking was reversed for a minimum of 4hrs at 65°C and DNA was purified with a QiaAmp DNA Micro Kit (QIAGEN) prior to real-time PCR.

RNA Analysis

Total RNA extraction, cDNA synthesis, real-time PCR and gene expression profiling was performed as described previously (Bennecke et al., 2010). In gene set enrichment analysis (GSEA) we matched 94 "stem cell transcripts" (van der Flier et al., 2009) to all transcripts from the Affymetrix Mouse Genome 430A 2.0 Array, respectively. GSEA software is provided by Broad Institute of MIT and Harvard University (http://www.broad.mit.edu/gsea). We acknowledge the use of GSEA software (Subramanian et al., 2005) to validate correlation between molecular pathways signatures in any phenotype of interest. For analysis of gene sets we changed default parameters as follows: permutation number to 1,000; collapse data set to gene symbols if "false"; gene sets smaller than 1 and larger than 2,000 were excluded.

Statistical Analysis

Data are expressed as mean ± SEM. Differences were analyzed by log-rank or Student's t test with Prism4 (GraphPad Software). p values $\leq$ 0.05 were considered significant.

SUPPLEMENTAL INFORMATION

Supplemental Information includes four figures and can be found with this article online at http://dx.doi.org/10.1016/j.cell.2012.12.012.

ACKNOWLEDGMENTS

We thank Kristin Retzlaff, Saskia Ettl, and Kerstin Burmeister for technical assistance; Jörg Mages and Angela Servatius for generation of microarray data; and Matthias Schiemann for FACS sorting as well as Michael Allgäuer for help with in situ hybridization. We are grateful to Sylvie Robine for generously providing *villin-cre*ER^{T2} mice. We thank Bert Vogelstein and Kenneth Kinzler for providing β-catenin^{S33Y} and TCF4 plasmids as well as TOPFLASH and FOPFLASH reporter constructs. We also thank Masayuki Miura for providing ERAI-transgenic mice and the pCAX-F-XBP1ΔDBD-venus plasmid. This work was supported by grants from the European Research Council (ROSCAN-281967), Deutsche Forschungsgemeinschaft, and Deutsche Krebshilfe to F.R.G.

Received: August 17, 2011
Revised: June 12, 2012
Accepted: December 4, 2012
Published: December 27, 2012

REFERENCES

Barker, N., van Es, J.H., Kuipers, J., Kujala, P., van den Born, M., Cozijnsen, M., Haegebarth, A., Korving, J., Begthel, H., Peters, P.J., and Clevers, H. (2007). Identification of stem cells in small intestine and colon by marker gene Lgr5. Nature *449*, 1003–1007.

Barker, N., Ridgway, R.A., van Es, J.H., van de Wetering, M., Begthel, H., van den Born, M., Danenberg, E., Clarke, A.R., Sansom, O.J., and Clevers, H. (2009). Crypt stem cells as the cells-of-origin of intestinal cancer. Nature *457*, 608–611.

Barroca, V., Lassalle, B., Coureuil, M., Louis, J.P., Le Page, F., Testart, J., Allemand, I., Riou, L., and Fouchet, P. (2009). Mouse differentiating spermatogonia can generate germinal stem cells in vivo. Nat. Cell Biol. *11*, 190–196.

Batlle, E., Henderson, J.T., Beghtel, H., van den Born, M.M., Sancho, E., Huls, G., Meeldijk, J., Robertson, J., van de Wetering, M., Pawson, T., and Clevers, H. (2002). Beta-catenin and TCF mediate cell positioning in the intestinal epithelium by controlling the expression of EphB/ephrinB. Cell *111*, 251–263.

Bennecke, M., Kriegl, L., Bajbouj, M., Retzlaff, K., Robine, S., Jung, A., Arkan, M.C., Kirchner, T., and Greten, F.R. (2010). Ink4a/Arf and oncogene-induced senescence prevent tumor progression during alternative colorectal tumorigenesis. Cancer Cell *18*, 135–146.

Bienz, M., and Clevers, H. (2000). Linking colorectal cancer to Wnt signaling. Cell *103*, 311–320.

Bollrath, J., and Greten, F.R. (2009). IKK/NF-kappaB and STAT3 pathways: central signalling hubs in inflammation-mediated tumour promotion and metastasis. EMBO Rep. *10*, 1314–1319.

Brabletz, T., Jung, A., Spaderna, S., Hlubek, F., and Kirchner, T. (2005). Opinion: migrating cancer stem cells - an integrated concept of malignant tumour progression. Nat. Rev. Cancer *5*, 744–749.

Chaffer, C.L., Brueckmann, I., Scheel, C., Kaestli, A.J., Wiggins, P.A., Rodrigues, L.O., Brooks, M., Reinhardt, F., Su, Y., Polyak, K., et al. (2011). Normal and neoplastic nonstem cells can spontaneously convert to a stem-like state. Proc. Natl. Acad. Sci. USA *108*, 7950–7955.

Chen, L.W., Egan, L., Li, Z.W., Greten, F.R., Kagnoff, M.F., and Karin, M. (2003). The two faces of IKK and NF-kappaB inhibition: prevention of systemic inflammation but increased local injury following intestinal ischemia-reperfusion. Nat. Med. *9*, 575–581.

Cole, J.W., and McKalen, A. (1963). Studies on the Morphogenesis of Adenomatous Polyps in the Human Colon. Cancer *16*, 998–1002.

Deng, J., Miller, S.A., Wang, H.Y., Xia, W., Wen, Y., Zhou, B.P., Li, Y., Lin, S.Y., and Hung, M.C. (2002). beta-catenin interacts with and inhibits NF-kappa B in human colon and breast cancer. Cancer Cell *2*, 323–334.

Fearon, E.R. (2011). Molecular genetics of colorectal cancer. Annu. Rev. Pathol. *6*, 479–507.

Gidekel Friedlander, S.Y., Chu, G.C., Snyder, E.L., Girnius, N., Dibelius, G., Crowley, D., Vasile, E., DePinho, R.A., and Jacks, T. (2009). Context-dependent transformation of adult pancreatic cells by oncogenic K-Ras. Cancer Cell *16*, 379–389.

Greten, F.R., Eckmann, L., Greten, T.F., Park, J.M., Li, Z.W., Egan, L.J., Kagnoff, M.F., and Karin, M. (2004). IKKbeta links inflammation and tumorigenesis in a mouse model of colitis-associated cancer. Cell *118*, 285–296.

Grivennikov, S.I., Greten, F.R., and Karin, M. (2010). Immunity, inflammation, and cancer. Cell *140*, 883–899.

Guerra, C., Schuhmacher, A.J., Cañamero, M., Grippo, P.J., Verdaguer, L., Pérez-Gallego, L., Dubus, P., Sandgren, E.P., and Barbacid, M. (2007). Chronic pancreatitis is essential for induction of pancreatic ductal adenocarcinoma by K-Ras oncogenes in adult mice. Cancer Cell *11*, 291–302.

Guerra, C., Collado, M., Navas, C., Schuhmacher, A.J., Hernández-Porras, I., Cañamero, M., Rodriguez-Justo, M., Serrano, M., and Barbacid, M. (2011). Pancreatitis-induced inflammation contributes to pancreatic cancer by inhibiting oncogene-induced senescence. Cancer Cell *19*, 728–739.

Guma, M., Stepniak, D., Shaked, H., Spehlmann, M.E., Shenouda, S., Cheroutre, H., Vicente-Suarez, I., Eckmann, L., Kagnoff, M.F., and Karin, M. (2011). Constitutive intestinal NF-κB does not trigger destructive inflammation unless accompanied by MAPK activation. J. Exp. Med. *208*, 1889–1900.

Guo, W., Keckesova, Z., Donaher, J.L., Shibue, T., Tischler, V., Reinhardt, F., Itzkovitz, S., Noske, A., Zürrer-Härdi, U., Bell, G., et al. (2012). Slug and Sox9 cooperatively determine the mammary stem cell state. Cell *148*, 1015–1028.

Gupta, P.B., Chaffer, C.L., and Weinberg, R.A. (2009). Cancer stem cells: mirage or reality? Nat. Med. *15*, 1010–1012.

Hanahan, D., and Weinberg, R.A. (2011). Hallmarks of cancer: the next generation. Cell *144*, 646–674.

Harada, N., Tamai, Y., Ishikawa, T., Sauer, B., Takaku, K., Oshima, M., and Taketo, M.M. (1999). Intestinal polyposis in mice with a dominant stable mutation of the beta-catenin gene. EMBO J. *18*, 5931–5942.

Iwawaki, T., Akai, R., Kohno, K., and Miura, M. (2004). A transgenic mouse model for monitoring endoplasmic reticulum stress. Nat. Med. *10*, 98–102.

Jackson, E.L., Willis, N., Mercer, K., Bronson, R.T., Crowley, D., Montoya, R., Jacks, T., and Tuveson, D.A. (2001). Analysis of lung tumor initiation and progression using conditional expression of oncogenic K-ras. Genes Dev. *15*, 3243–3248.

Jaenisch, R., and Young, R. (2008). Stem cells, the molecular circuitry of pluripotency and nuclear reprogramming. Cell *132*, 567–582.

Janssen, K.P., Alberici, P., Fsihi, H., Gaspar, C., Breukel, C., Franken, P., Rosty, C., Abal, M., El Marjou, F., Smits, R., et al. (2006). APC and oncogenic KRAS are synergistic in enhancing Wnt signaling in intestinal tumor formation and progression. Gastroenterology *131*, 1096–1109.

Karin, M., and Greten, F.R. (2005). NF-kappaB: linking inflammation and immunity to cancer development and progression. Nat. Rev. Immunol. *5*, 749–759.

Kaser, A., Lee, A.H., Franke, A., Glickman, J.N., Zeissig, S., Tilg, H., Nieuwenhuis, E.E., Higgins, D.E., Schreiber, S., Glimcher, L.H., and Blumberg, R.S. (2008). XBP1 links ER stress to intestinal inflammation and confers genetic risk for human inflammatory bowel disease. Cell *134*, 743–756.

Nagashima, K., Sasseville, V.G., Wen, D., Bielecki, A., Yang, H., Simpson, C., Grant, E., Hepperle, M., Harriman, G., Jaffee, B., et al. (2006). Rapid TNFR1-dependent lymphocyte depletion in vivo with a selective chemical inhibitor of IKKbeta. Blood *107*, 4266–4273.

Perkins, N.D. (2012). The diverse and complex roles of NF-κB subunits in cancer. Nat. Rev. Cancer *12*, 121–132.

Polyak, K., and Weinberg, R.A. (2009). Transitions between epithelial and mesenchymal states: acquisition of malignant and stem cell traits. Nat. Rev. Cancer *9*, 265–273.

Preston, S.L., Wong, W.M., Chan, A.O., Poulsom, R., Jeffery, R., Goodlad, R.A., Mandir, N., Elia, G., Novelli, M., Bodmer, W.F., et al. (2003). Bottom-up histogenesis of colorectal adenomas: origin in the monocryptal adenoma and initial expansion by crypt fission. Cancer Res. *63*, 3819–3825.

Rothwell, P.M., Fowkes, F.G., Belch, J.F., Ogawa, H., Warlow, C.P., and Meade, T.W. (2011). Effect of daily aspirin on long-term risk of death due to cancer: analysis of individual patient data from randomised trials. Lancet *377*, 31–41.

Rupec, R.A., Jundt, F., Rebholz, B., Eckelt, B., Weindl, G., Herzinger, T., Flaig, M.J., Moosmann, S., Plewig, G., Dörken, B., et al. (2005). Stroma-mediated dysregulation of myelopoiesis in mice lacking I kappa B alpha. Immunity *22*, 479–491.

Saccani, S., Pantano, S., and Natoli, G. (2003). Modulation of NF-kappaB activity by exchange of dimers. Mol. Cell *11*, 1563–1574.

Sangiorgi, E., and Capecchi, M.R. (2008). Bmi1 is expressed in vivo in intestinal stem cells. Nat. Genet. *40*, 915–920.

Sansom, O.J., Meniel, V., Wilkins, J.A., Cole, A.M., Oien, K.A., Marsh, V., Jamieson, T.J., Guerra, C., Ashton, G.H., Barbacid, M., and Clarke, A.R. (2006). Loss of Apc allows phenotypic manifestation of the transforming properties of an endogenous K-ras oncogene in vivo. Proc. Natl. Acad. Sci. USA *103*, 14122–14127.

Sato, T., Vries, R.G., Snippert, H.J., van de Wetering, M., Barker, N., Stange, D.E., van Es, J.H., Abo, A., Kujala, P., Peters, P.J., and Clevers, H. (2009). Single Lgr5 stem cells build crypt-villus structures in vitro without a mesenchymal niche. Nature *459*, 262–265.

Shibata, H., Toyama, K., Shioya, H., Ito, M., Hirota, M., Hasegawa, S., Matsumoto, H., Takano, H., Akiyama, T., Toyoshima, K., et al. (1997). Rapid colorectal adenoma formation initiated by conditional targeting of the Apc gene. Science *278*, 120–123.

Shih, I.M., Wang, T.L., Traverso, G., Romans, K., Hamilton, S.R., Ben-Sasson, S., Kinzler, K.W., and Vogelstein, B. (2001). Top-down morphogenesis of colorectal tumors. Proc. Natl. Acad. Sci. USA *98*, 2640–2645.

Spiegelman, V.S., Slaga, T.J., Pagano, M., Minamoto, T., Ronai, Z., and Fuchs, S.Y. (2000). Wnt/beta-catenin signaling induces the expression and activity of betaTrCP ubiquitin ligase receptor. Mol. Cell *5*, 877–882.

Subramanian, A., Tamayo, P., Mootha, V.K., Mukherjee, S., Ebert, B.L., Gillette, M.A., Paulovich, A., Pomeroy, S.L., Golub, T.R., Lander, E.S., and Mesirov, J.P. (2005). Gene set enrichment analysis: a knowledge-based

approach for interpreting genome-wide expression profiles. Proc. Natl. Acad. Sci. USA *102*, 15545–15550.

Tian, H., Biehs, B., Warming, S., Leong, K.G., Rangell, L., Klein, O.D., and de Sauvage, F.J. (2011). A reserve stem cell population in small intestine renders Lgr5-positive cells dispensable. Nature *478*, 255–259.

van de Wetering, M., Sancho, E., Verweij, C., de Lau, W., Oving, I., Hurlstone, A., van der Horn, K., Batlle, E., Coudreuse, D., Haramis, A.P., et al. (2002). The beta-catenin/TCF-4 complex imposes a crypt progenitor phenotype on colorectal cancer cells. Cell *111*, 241–250.

van der Flier, L.G., van Gijn, M.E., Hatzis, P., Kujala, P., Haegebarth, A., Stange, D.E., Begthel, H., van den Born, M., Guryev, V., Oving, I., et al. (2009). Transcription factor achaete scute-like 2 controls intestinal stem cell fate. Cell *136*, 903–912.

Vlantis, K., Wullaert, A., Sasaki, Y., Schmidt-Supprian, M., Rajewsky, K., Roskams, T., and Pasparakis, M. (2011). Constitutive IKK2 activation in intestinal epithelial cells induces intestinal tumors in mice. J. Clin. Invest. *121*, 2781–2793.

Wagner, M., Greten, F.R., Weber, C.K., Koschnick, S., Mattfeldt, T., Deppert, W., Kern, H., Adler, G., and Schmid, R.M. (2001). A murine tumor progression model for pancreatic cancer recapitulating the genetic alterations of the human disease. Genes Dev. *15*, 286–293.

Yochum, G.S., McWeeney, S., Rajaraman, V., Cleland, R., Peters, S., and Goodman, R.H. (2007). Serial analysis of chromatin occupancy identifies beta-catenin target genes in colorectal carcinoma cells. Proc. Natl. Acad. Sci. USA *104*, 3324–3329.

Cell

SUPPLEMENTAL REFERENCE

Iwawaki, T., Akai, R., Kohno, K., and Miura, M. (2004). A transgenic mouse model for monitoring endoplasmic reticulum stress. Nat. Med. *10*, 98–102.

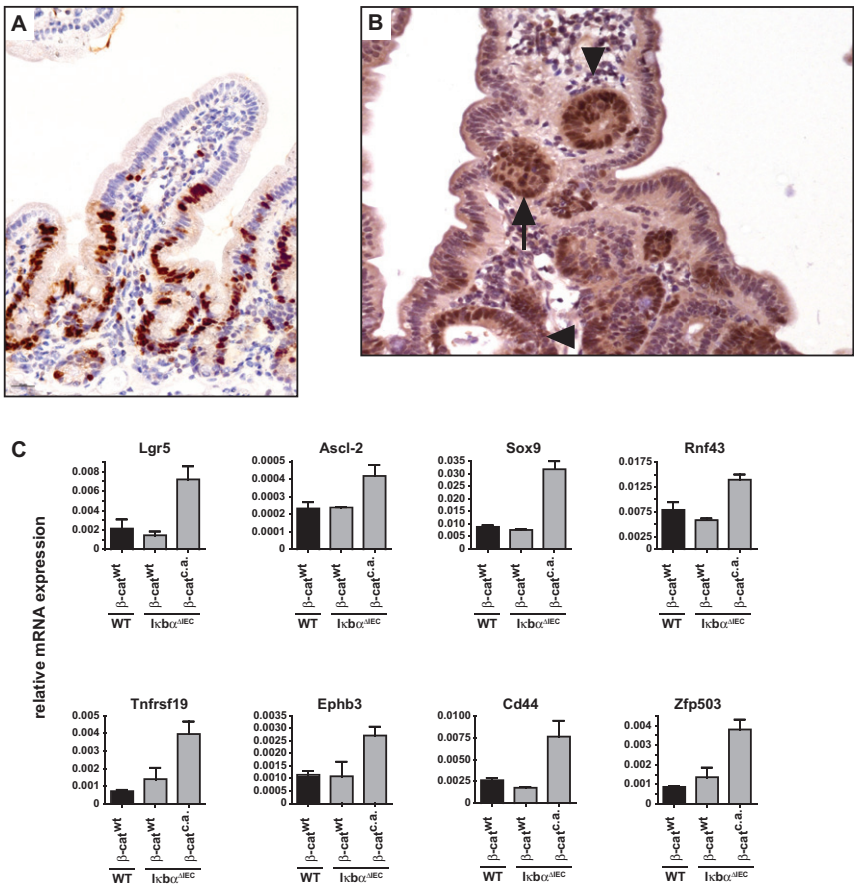

Figure S1. Crypt-Like Structures Can Be Found within 24 Hours in *β-cat*$^{c.a.}$/*Ikba*$^{\Delta IEC}$ Mice, but Loss of *Ikba* Alone Is Not Sufficient to Upregulate Stem Cell Markers in IEC, Related to Figure 4

(A) Crypt-like structure expressing BrdU in upper villi occur in *β-cat*$^{c.a.}$/*Ikba*$^{\Delta IEC}$ mice within 24 hr after tamoxifen administration.

(B) Immunohistochemial analysis of c-*myc*-expressing adenomatous crypts (arrowheads) in the subepithelium of *β-cat*$^{c.a.}$/*Ikba*$^{\Delta IEC}$ villi. Arrow indicates crypt-like structure that is in the process of invading into the subepithelium.

(C) Relative mRNA expression of intestinal stem cell markers in IEC of WT, *Ikba*$^{\Delta IEC}$ and *β-cat*$^{c.a.}$/*Ikba*$^{\Delta IEC}$ mice analyzed by Real-Time PCR. Data are mean ± SE, n ≥ 3.

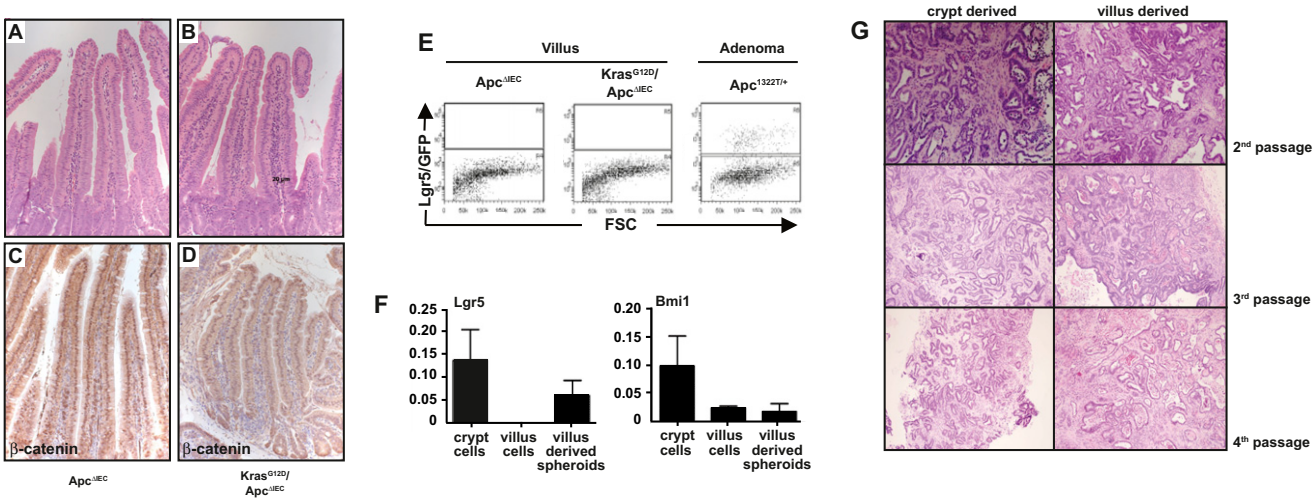

Figure S2. Lack of Lgr5$^+$ Cells in In Villus Fractions Used for Organoid Cultures, Related to Figure 5

(A–D) Comparable morphological appearance and nuclear expression of β-catenin (C, D) in *Apc$^{\Delta IEC}$* (A, C) and *Apc$^{\Delta IEC}$/K-ras^{G12D}* (B, D) mice 2 days after a single dose of tamoxifen.

(E) FACS analysis confirms absence of Lgr5+ cells in villus fractions used for organoid culture. *Apc$^{\Delta IEC}$* and *Apc$^{\Delta IEC}$/K-ras^{G12D}* mice had been crossed to *Lgr5-EGFP-IRES- creERT2* animals to allow sorting of Lgr5$^+$ cells based on EGFP expression. Adenomas from *Lgr5-EGFP-IRES-creER^{T2}/Apc^{1322T}* mice were used as positive controls.

(F) PCR of Lgr5 and Bmi1 confirms absence of Lgr5 in isolated villus cells and re-expression of Lgr5 in villus-derived spheroids. In contrast, low levels of Bmi1 were detectable in villus preparations, however, these did not further increase in spheroids. Data are mean ± SE, n ≥ 3.

(G) Comparable histology of tumors that grew subcutaneously in CD1 athymic mice independently of spheroid passage or whether spheroids were derived from crypts or villus preparations.

Similar results were obtained when villus cells were isolated 6 hr after tamoxifen administration in *Apc$^{\Delta IEC}$/K-ras^{G12D}* mice.

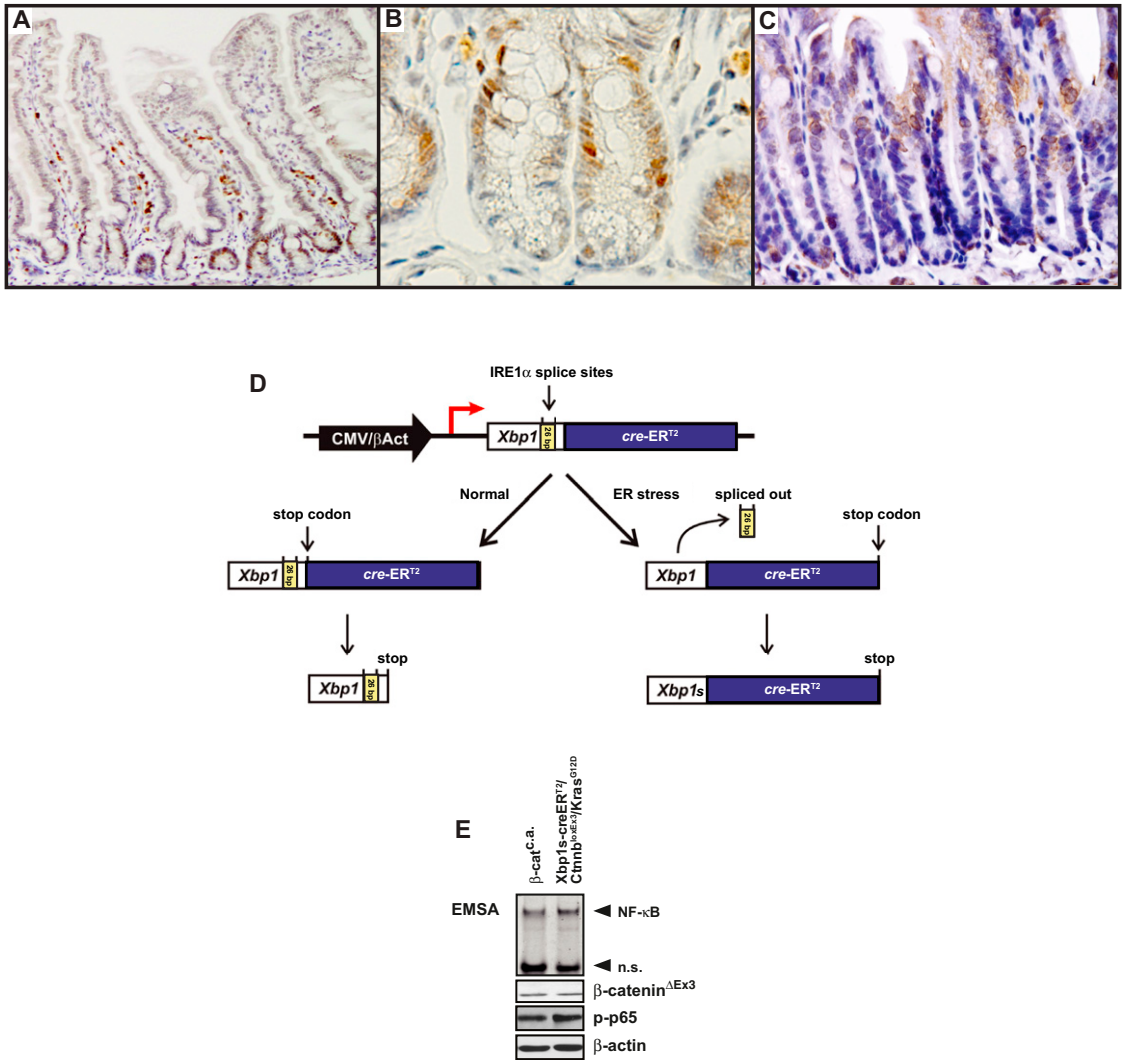

Figure S3. Constitutive Splicing of Xbp in Nonstem Cells Allows Recombination in Lgr5$^-$ and Bmi1$^-$ IEC, Related to Figure 6

(A and B) Immunohistochemial analysis of Xbp in WT mice. Note that only IEC known to be Lgr5$^-$ at the crypt villus junction, in the transit amplifying compartment and Paneth cells stain positive.

(C) Immunohistochemical staining of GFP in unchallenged ER stress-activated indicator mice (ERAI-mice)(Iwawaki et al., 2004) that drive expression of venus (a variant of green fluorescent protein) in response to Xbp splicing. Interestingly, GFP expression in IEC of untreated mice reveals constitutive Xbp splicing. We therefore reasoned that this observation would allow targeted expression of cre-ERT2 in Lgr5$^-$ IEC, but not in Lgr5$^+$ cells.

(D) The construct that was initially used to generate ERAI mice (generously provided by M. Miura) was used to replace the coding sequence of venus with a cre-ER^{T2} sequence, so cre-ER^{T2} expression would be achieved only in cells that splice Xbp (C). The fact that Lgr5$^-$ IEC revealed spontaneous Xbp splicing allowed cre expression without exogenous induction of ER stress.

(E) EMSA and immunoblot analysis demonstrates elevated NF-κB activation and comparable expression of exon3 deleted β-catenin in *Xbp1s-cre*ER^{T2}/*Ctnnb*^{loxEx3}/*K-ras*^{G12D} mice compared to *β-cat*$^{c.a}$ mice.

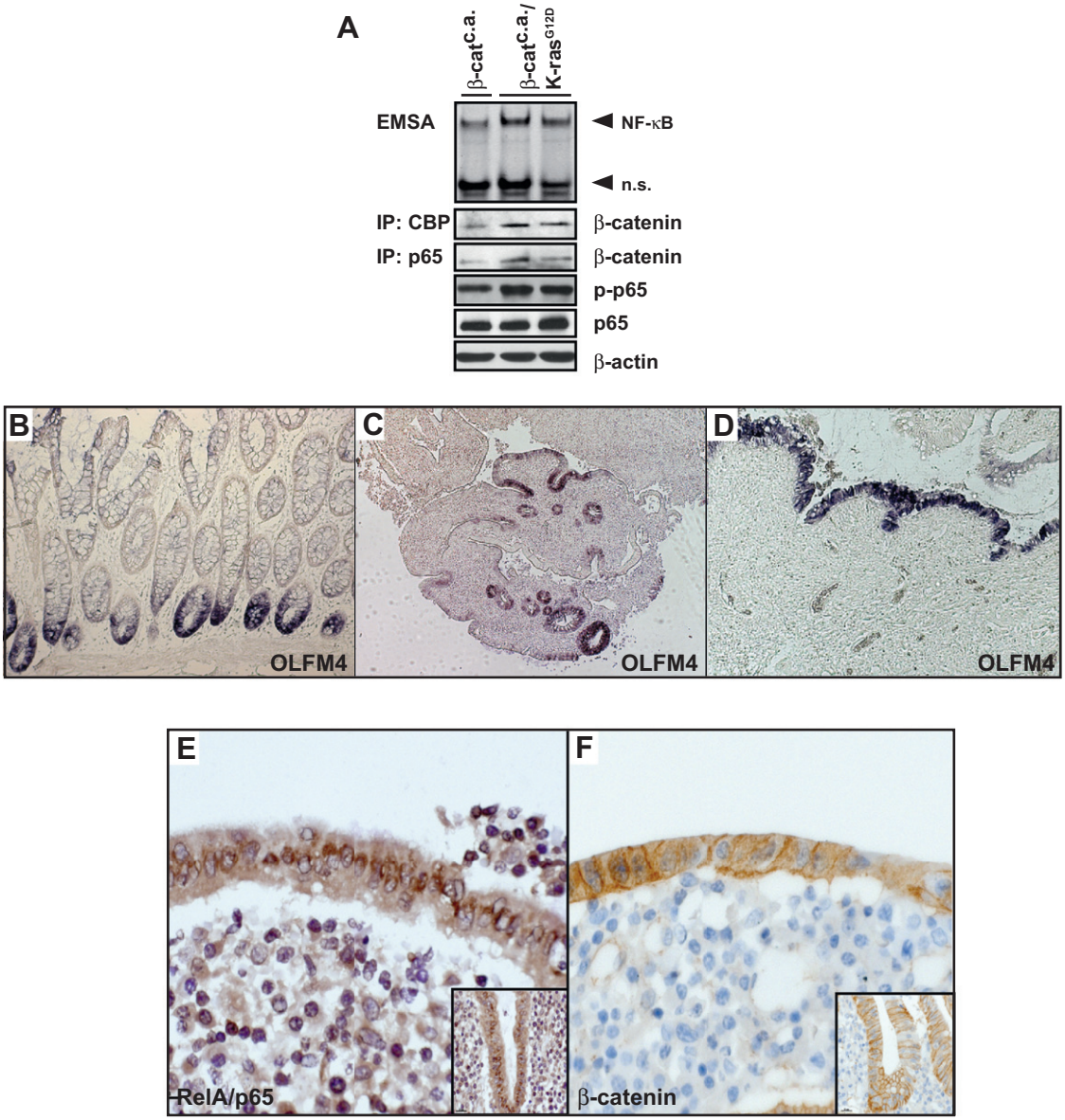

Figure S4. Expansion and Aberrant Localization of Stem Cells in the Colon of Ulcerative Colitis Patients, Related to Figure 7

(A) EMSA and immunoblot analysis demonstrates elevated NF-κB activation and increased interaction between CBP and β-catenin as well as RelA/p65 and β-catenin in IEC from *β-cat*$^{c.a}$/K-ras^{G12D} mice animals compared to *β-cat*$^{c.a}$ mice.

(B–D) In situ hybridization with a probe specific for the stem cell marker OLFM4 in human healthy mucosa (B) and in ulcerative colitis patients (C and D). Whereas in healthy mucosa expression is restricted to cells at the bottom of colonic crypts, during ulcerative colitis expression is expanded and can be found outside of crypts especially in IEC that cover ulcerations.

(E and F) Immunohistochemical staining of RelA/p65 (E) and β-catenin (F) in ulcerative colitis patients and healthy mucosa (small inset).